SDL-15-NGL 34-002-098

THE ELECTRICAL PROPERTIES OF 60 KEV ZINC IONS IMPLANTED INTO SEMI-INSULATING GALLIUM ARSENIDE

NASA GRANT NGL 34-002-098

May 1972

M. A. Littlejohn
Rangappan Anikara

Solid State Device Laboratory
Department of Electrical Engineering
North Carolina State University
Raleigh, N. C. 27607

ABSTRACT

RANGAPPAN, ANIKARA. The Electrical Properties of 60 KeV Zinc Ions Implanted into Semi-insulating Gallium-Arsenide (under the direction of Michael A. Littlejohn).

The electrical behavior of zinc ions implanted into chromium doped semi-insulating gallium-arsenide has been investigated by measurements of the sheet resistivity and Hall-effect. Room temperature implantations have been performed using fluence values from 1×10^{12} /cm^2 to 1×10^{15} /cm^2 at 60 KeV. The samples were annealed for 30 minutes in a nitrogen atmosphere up to 800°C in steps of 200°C and the effect of this annealing on the Hall-effect and sheet resistivity has been studied at room temperature using the well-known Van der Pauw technique.

The temperature dependence of sheet resistivity and mobility was measured from liquid nitrogen temperature to room temperature. Finally, a measurement of the implanted profile was obtained using a layer removal technique combined with the Hall-effect and sheet resistivity measurements. This measurement was made on a sample implanted with a dose of 1×10^{15} /cm^2.

The implanted layers were all p- type in the as - implanted condition before annealing. For ion doses between 1×10^{12} /cm^2 to 1×10^{14} /cm^2 the mobility and sheet resistivity increased drastically upon annealing to 400°C. In the range between 600°C to 800°C the mobility value saturated and the resistivity decreased, bringing the electrically active effective surface concentration near the total dose. The samples with heavier doses behaved in the

same way as far as mobility was concerned. However, the resistivity continually decreased with annealing temperature, and the effective carrier concentration was far below the total dose.

The results of the temperature dependence of the resistivity and mobility show that a deep-lying defect center predominates the electrical transport properties. An estimate of the activation energy of this defect is 0.26eV above the valence band edge. An estimate of the implanted profile indicates that enhanced diffusion during annealing is occurring and that the defect centers could be compensating donors in nature.

TABLE OF CONTENTS

LIST OF FIGURES

CHAPTER I

1. INTRODUCTION

Ion implantation is the introduction of atoms into the surface layer of a solid substrate by bombardment of the solid with ions in the KeV to MeV energy range.

As a means of doping semiconductors, ion implantation has been a subject of considerable interest in recent years. This is because it is an intriguing physical process as well as having the practical possibilities of improved or unique methods for making semiconductor devices. Some of the characteristics of ion implantation which are of potential value are lower process temperatures and the possibility of attaining doping concentrations well above the solid solubility limit in thin layers. With respect to masking, special advantages include the use of evaporated or demountable metal masks and the possibility of eliminating masks by doping patterns directly with programmed ion beams. In contrast to the diffusion process, an important aspect of the application of ion implantation to semiconductor technology is that the number of implanted ions is controlled by the external system rather than the physical properties of the substrate.

The physical processes taking place during ion implantation are much more complex than those occurring during thermal diffusion. The energy of the incident ion is more than five orders of magnitude larger than the thermal energies used in diffusion. Because of the high energy of the incident ion, a substantial amount of lattice disorder is produced. The influence of the semiconductor lattice

on the path of the ion is another important complicating factor. As a result the number of process parameters influencing the final electrical behavior of the implanted layer is far greater than for the diffusion process.

In tracing the ion to its final location in the crystal, a number of processes must be considered. An ion can lose its energy in several ways. Those ions which either impinge on, or are deflected into, paths that do not lie along a low order crystallographic direction lose their energy as predicted by the Linhard, Scharff and Schiott (L.S.S.) theory (15) for the stopping of heavy ions in an amorphous substrate. The density distribution predicted by the L.S.S. theory depends upon the energy of the incident ion, its mass, the total dose and the mass of the substrate atom. Other ions either impinge on, or are deflected into, paths that do lie along a low index crystallographic direction. These ions are steered or channeled along that direction. This results in reduced energy loss of these ions and a corresponding deeper penetration. In the density distribution, a second peak at a greater depth indicates the channeled ions. In most cases, however, the channeled ions, tend to escape from the channel as the result of collisions with imperfections and the distribution is dispersed.

When the ion comes to rest, it may occupy any one of several positions in the lattice. These include substitutional sites, regular interstitial sites, non-regular interstitial sites, or precipitation sites. The type of site is of importance to the subsequent behavior of the ion, both during the remainder of the implant and the subsequent annealing cycle. The type of site occupied also determines the electrical behavior of an ion. The distribution of the ions among the possible lattice sites can

be strongly influenced by all the implant conditions, including the incident ion species and energy, substrate composition, temperature, crystal structure, and orientation of the beam with respect to the substrate. This distribution of the ions among the possible lattice sites is closely related to the type and spatial distribution of the disorder which the ions produce as they lose their energy to the lattice. A typical example of such a situation is in thallium-implanted silicon at 450°C (19). After a room temperature implant, 30% of the implanted atoms were on regular interstitial sites and another 30% on substitutional sites. The authors (19) have measured only 60% of the total implanted atoms and nothing is mentioned about the remaining 40% . Upon annealing, the substitutional component decreased and the interstitial level showed a corresponding increase, indicating that the substitutional atoms were moving to interstitial sites. Finally, at high annealing temperatures, the interstitial level decreased as the implanted ions moved to non-regular lattice sites, such as precipitation centers.

The maximum substrate temperatures encountered in ion implantation are comparatively low. However, diffusion plays an important role in determining the eventual distribution of the implanted ions after high temperature anneals, which are almost always necessary to remove radiation damage. During implantation diffusion of the implanted atoms can also occur, and can be enhanced by the presence of lattice vacancies, substrate interstitials, and dopant interstitials which are present in much higher concentrations than in the case of thermal equilibrium (8). During subsequent annealing, enhanced diffusion can take place. The annealing of the disordered regions can release vacancies, substrate

interstitials, and dopant interstitials maintaining concentrations that are again much greater than those which would result in thermal equilibrium. This diffusion results in a "spreading out" of the distribution and can lead to the movement of junctions and loss of dopant ions to the surface or to precipitation sites. At sufficiently high annealing temperatures, thermal equilibrium is approached and the influence of the solid solubility can become apparent.

Thus, the electrical behavior of an implanted layer is affected by a number of factors. Ion implantation of silicon and germanium have been studied rather extensively by several authors (1, 13, 17) especially by Davis et. al. (6) at the Chalk River Laboratories. Several types of measurement techniques have been used to study the behavior of the implanted species. Some of these techniques are:

1. Rutherford scattering studies. This involves the studying of the orientation dependence of the back scattering yield of approximately 1.0 MeV helium ions. This gives an idea of the lattice disorder produced and the location of the implanted ions.
2. Radio Tracer method. In this method the target is implanted with radioactive ions. Then the depth distribution of the embedded radioactivity is determined by removing a series of thin uniform layers from the surface of the substrate, and measuring the residual activity after each layer removal. This gives the implanted profile of the atomic species and not the electrically active centers.
3. Hall-Effect and sheet-resistivity measurements: These measurements combined with layer removal techniques are used in determining the effective surface carrier concentration, the effective mobility, and

the implanted profile. The temperature dependence of the same parameters sheds more light on the nature of the transport properties.

4. Capacitance-Voltage characteristics. The capacitance-voltage characteristics of surface barriers formed on donor implanted n-type material or acceptor implanted p-type material determines the profile of the active centers.
5. Diode studies. By compound implantations diodes are formed. Their voltage-current characteristics and optical luminescence characteristics, if applicable, are studied. By angle sectioning and staining techniques the measurement of the junction depth is made for different doses which enables one to determine the profile and electrical nature of the implanted atom.

Presently, implanted layers in III-V compound semiconductors are not nearly as well characterized as those in silicon and germanium. The III-V compound semiconductors have efficient laser and electroluminescent properties as well as other desirable properties for device applications. Before characterizing the properties of implanted layers for such applications the substrate system itself should be well-characterized and understood. Among the compound semi conductors, gallium-arsenide is probably the most thoroughly investigated material and should offer a desirable substrate for studying ion implantation as a doping process in III-V compound semiconductors.

The aim of this thesis is to study the electrical properties of the p-type layer produced in semi-insulating gallium-arsenide by the implantation of zinc ions. Doping gallium-arsenide by thermal diffusion

is complicated. The substrate and the dopant have to be encapsulated in a spectrosil quartz tube and they have to be maintained in different temperature zones. Special care must be taken to reduce arsenic loss. Ion implantation doping overcomes many of the difficulties of thermal diffusion and is an elegant method of doping gallium-arsenide. Among the five techniques previously described to study the nature of the implanted layer or device, only the resistivity and Hall-effect measurements reveal the bulk electrical properties. Hence, this method was chosen. The sheet-resistivity and Hall-effect measurements at room temperature were made to determine the annealing characteristics of the zinc implanted gallium-arsenide. These measurements as a function of temperature revealed the nature of the carriers and the same measurements combined with etching of thin layers yielded a rough estimate of the post annealed profile of active centers.

CHAPTER II

2. REVIEW OF LITERATURE

2.1 Implanted Layers in Low-Resistivity Gallium-Arsenide.

Gallium-arsenide is probably the most widely studied and well-characterized of the compound semiconductors. Presently, most of the studies of the properties of ion implanted layers in gallium-arsenide have been made using low resistivity substrates (4, 7, 9, 10, 11, 12, 16, 18, 20 and 29). These studies can be classified into radiation damage and bulk electrical properties studies. The references cited are not all inclusive. However, they do give an idea of the present state of affairs for implantations into low resistivity gallium-arsenide substrates.

Extensive radiation damage studies have been done by O. J. Marsh et. al. (17) and T. E. Westmoreland et. al. (29). They have investigated the lattice disorder produced in gallium-arsenide by 60 KeV cadmium and 70 KeV zinc ion implantations. Rutherford back scattering studies of 1·0 MeV helium ion beams were conducted in order to establish the relative amounts of lattice disorder present in samples and for identifying the location of the implanted ions. The back scattering studies with the helium ion beam were found to be time consuming. The critical alignment of the sample with the analysis beam was found to be an especially difficult and time consuming problem. In order to do a rapid qualitative analysis two methods were employed. One used a scanning electron microscope and the other a spectrophotometer. The scanning electron microscope was used to display the secondary (or back

scattered) electron intensity as a function of the angle of incidence of the electron beam on a single crystal surface (17). The patterns obtained are similar to Kikuchi diffraction patterns. The quality of the Coates-Kikuchi patterns is sensitive to any chemical or physical process which tend to disturb the periodicity of the first few hundred angstroms of the crystal surface. The intensity patterns from the implanted substrate and the unimplanted substrate were compared, and the change in the intensity was taken as a measure of the damage produced due to implantation. In a similar manner reflectance measurements were made with a double beam spectrophotometer using a specular reflectance attachment. The fractional change in the intensity at the reflectance peak (2450Å) was taken as the measure of damage.

The results of the radiation damage studies by O. J. Marsh et. al. (17) and J. E. Westmoreland et. al. (29) are summarized as follows. There was no apparent difference between the anneal behavior of zinc and cadmium implants. The amount of disorder produced increased linearly with dose and saturated at a dose of approximately 1-2 x 10^{13} cadmium /cm^2. The disorder present in low dose implants ($\sim$ 5 x 10^{12} /cm^2) annealed appreciably by 150°C. With increasing doses of zinc or cadmium the samples showed a continuous increase in the anneal temperature required to remove a substantial amount of lattice disorder. For a 1 x 10^{15} /cm^2 dose more than 450°C annealing for 10 minutes was required. The correcpondence between the three previously mentioned methods was acceptable.

Carter et. al. (4) have investigated the anneal behavior of tellurium implanted gallium-arsenide at 40 KeV. According to

their studies a dose of 1 x 10^{15} tellurium /cm^2 disordered the material to the saturation level and a 500°C anneal was required to completely remove the damage.

O. J. Marsh et. al. have done extensive ion implantation studies in gallium-arsenide and have summarized their results (9, 17, 18), apart from several of their publications (10, 11, 12, 20, and 29). They have described the electrical properties of zinc, cadmium, tellurium and sulfur ions implanted at 400°C substrate temperature (9, 18) and room temperature implantations of carbon, sulfur and zinc ions (17, 18). In all these implantations the substrate used was n- or p- type, depending on the implantation species, having doping levels of about 10^{14} -$10^{16}/cm^3$. Zinc and cadmium implants produced p- type layers while sulfur, tellurium and selenium resulted in n- type layers. Since zinc implanted into semi-insulating gallium-arsenide is studied in this thesis, the work and results on zinc, in particular, is summarized below.

A number of low resistivity (1 ohm-cm) n- type gallium-arsenide samples were implanted with zinc ions at various fluence levels from 1 x 10^{13} /cm^2 to 1 x 10^{16} /cm^2. For 20 KeV implantations three different substrate temperatures of 500°C, 400°C and room temperature were maintained (11, 17). Also, 70 KeV implantations were made at 400°C and an 85 KeV implantation was made at room temperature (17, 10). In the 85 KeV and 70 KeV implants no p- type layer was formed until the samples were annealed to a high temperature (600°C for ion dose $\leq$ $10^{14}/cm^2$, 500°C for ion dose $\geq$ $10^{15}/cm^2$). However, the 20 KeV implants showed a p- type layer as implanted at 400°C or when annealed at 300°C for the room-

temperature implants. The annealing behavior of a 20 KeV zinc implant at 400°C with a $10^{16}/cm^2$ dose is reproduced in Figure 2.1. Figure 2.2. gives the sheet resistivity behavior of different doses of 20 KeV zinc implant at room temperature. The authors report that the data points for mobility and carrier concentration are widely scattered except for a $1 \times 10^{16}/cm^2$ dose.

From Figure 2.1. the effect of 10 minute annealings from 500°C to 900°C on a 20 KeV zinc implant made at 400°C is noted. Below 700°C the sheet resistivity decreased monotonically as a result of increasing mobility. Above 700°C the decrease was a result of increasing carrier concentration. In the temperature range below 700°C the surface carrier concentration first increased and then decreased somewhat with further annealing. The increase was thought to result from implanted ions moving to electrically active substitutional positions in the lattice. The decrease was not well understood and has been attributed to a number of possible causes. Compensation by defect centers which are released when damage clusters dissociate upon annealing and the variation of mobility with depth were attributed as the cause for the decrease in surface carrier concentration. The p-type layers obtained by 70 KeV zinc implants at 400°C were thought to be superior in electrical quality compared to the layers produced by the 20 KeV implant (18). For example, when annealed at 600°C for 2 minutes, a 70 KeV implant made at 400°C produced a layer with ρ_s=598 ohm/sq, μ=45.8 cm^2/V-sec, and N_s=2.28 x 10^{14} $/cm^2$. The corresponding values for a 20 KeV implanted sample were P_s=3100 ohm/sq, μ=13.5 cm^2/V-sec and N_s= 1.05 x $10^{14}/cm^2$. The increased

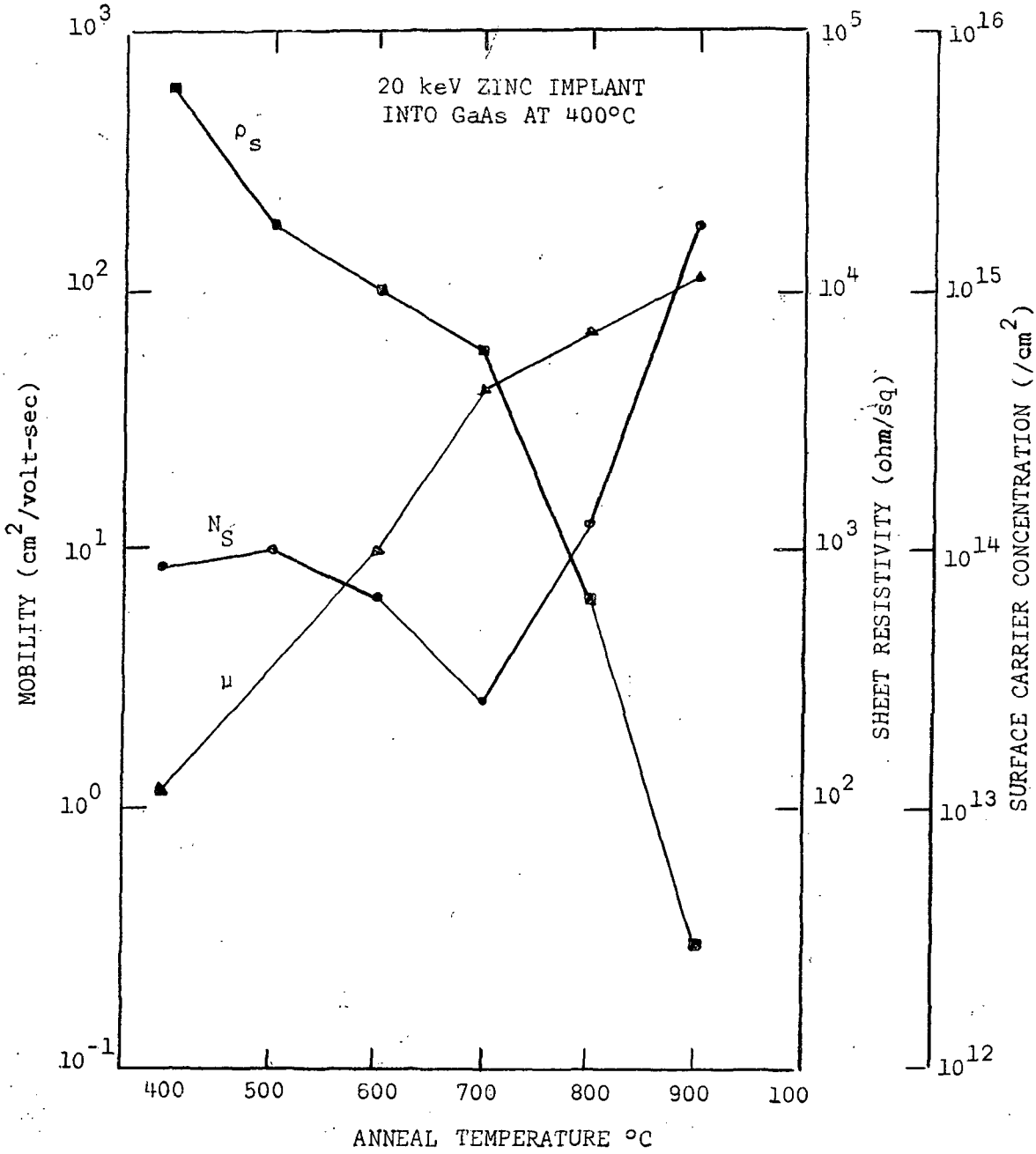

Figure 2.1. Effect of isochronal (10 min) anneals on zinc implanted gallium-arsenide.

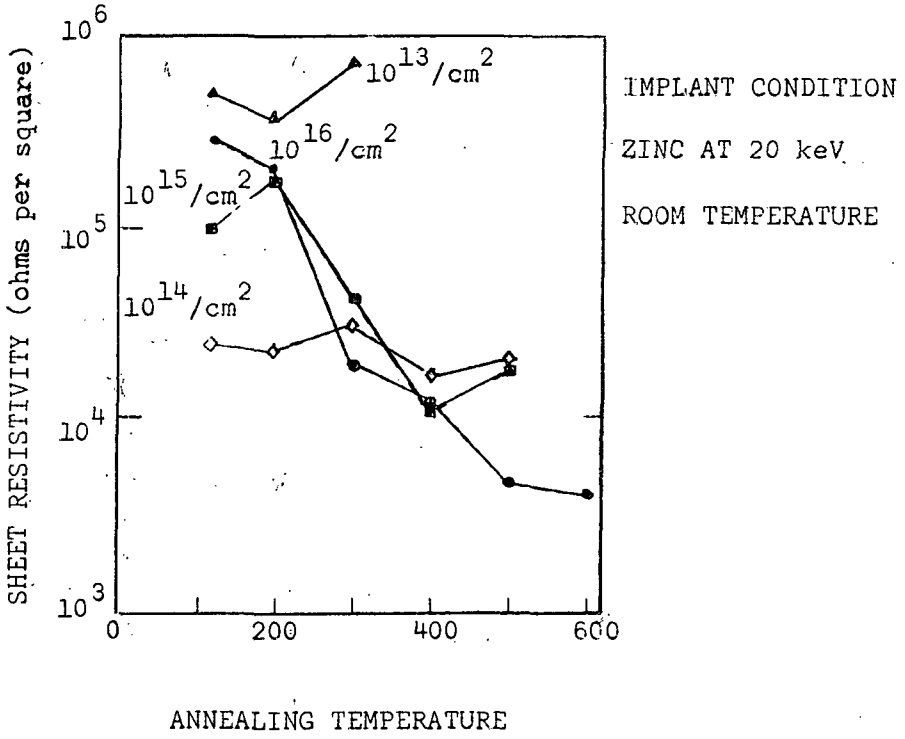

Figure 2.2. Dependence of sheet resistivity on anneal temperature - 20 keV zinc ion implanted layers.

mobility and reduced sheet resistivity of the 70 KeV implanted layer was attributed to the fact that most of the dopant ions were located deep within the semiconductor crystal and were thus less affected by surface defects. Measurement was made on only one sample to locate the junction by differential weight measurements using a slow etch. It was found that the major part of the implanted layer was less than 0•1μ deep in a 20 KeV implanted sample after 10 minute annealing at 600°C. Diodes produced by zinc implantation into n- type substrates exhibited good rectification characteristics with an unusually low leakage current of 10^{-8}A at 10 V reverse bias at room temperature. The electroluminescent spectrum of these diodes contained an emission peak which appeared to be associated with vacancy complexes, as well as a band emission peak.

Many workers have studied the electrical properties of elements other than zinc implanted into gallium-arsenide. The behavior of cadmium, sulfur, tin and selenium implants into low resistivity gallium-arsenide are summarized below.

The cadmium implants behaved in a similar manner to zinc implants except that the mobility of the cadmium implanted layer decreased after 800°C annealing. This was attributed to the low diffusion coefficient of cadmium compared to zinc. The main difference between cadmium and zinc was the enhanced post-implantation annealing diffusion. Cadmium implanted samples required relatively higher annealing temperatures compared to zinc implanted samples to achieve equivalent values of sheet resistivity and mobilities (18).

Sulfur implants into p-type substrates (12) behaved in a very

similar manner to zinc implants. There was considerable diffusion during annealing at high temperatures. The samples were n-type even before annealing. Tin implantations by the same authors failed to show an n- type layer even after 16-hours of annealing.

Foyt et. al. (7) have reported the most efficient implantation of selenium ions into p- type substrates. The efficiency of implantation (defined as the ratio of total implanted atoms to electrically active atoms) is reported as 50%. Mobility values of 1500 - 2000 $cm^2/V\text{-sec}$ and carrier concentrations of $1 \times 10^{19}/cm^3$ are reported for the selenium implantation.

2.2 Implanted Layers in Semi-insulating Gallium-Arsenide

Most of the above studies have been made using low resistivity gallium-arsenide. There are relatively few studies available which have been made using semi-insulating gallium-arsenide. Sansbury and Gibbons (24,25) have reported that silicon and sulfur behaved as donors and that carbon behaved as an acceptor when implanted into chromium doped semi-insulating gallium-arsenide. The substrate used had approximately 10^{16} donors/cm^3 introduced during growth. Chromium is present to a likely concentration of around $5 \times 10^{16}/cm^3$ and can be modeled as a deep acceptor approximately 0.79 eV from the conduction band. These deep lying acceptors compensate the donors which are almost equal in number. The resulting resistivity was 10^8 ohm-cm. With sample thicknesses of less than 500μ, this implies a sheet resistivity of $2 - 4 \times 10^9$ ohm/square. The ion energies used were combinations in the range of 10 to 70 KeV with doses between $10^{12}/cm^2$ to $10^{16}/cm^2$. Before annealing the resistivity of the implanted layers were consider-

ably below the substrate value, typically 10^5 ohm/square. This conductivity was presumed due to radiation damage. Hall-voltage measurements were not possible until after the samples were annealed at 550°C. The sheet resistivity increased with annealing and approached its maximum value for annealing temperatures between 400°C and 500°C. The maximum sheet resistivity was within an order of the substrate sheet resistivity. A significant annealing stage was found to occur at 600°C which considerably increased the mobility and carrier concentration. The mobility monotomically increased up to 650°C and then saturated. The carrier concentration steadily increased up to 750°C. A further increase in anneal temperature produced different effects in different samples. After a 700°C anneal, the electrical properties were comparable to those in bulk gallium-arsenide. For silicon implants, mobility values of 2700 cm^2/volt-sec, and for sulfur, mobility values of 3600 cm^2/volt-sec, are reported. For the p-type carbon implanted layers mobility values of 240 to 360 cm^2/volt-sec were noted. A doping efficiency of 11% for silicon and 2% for carbon were noted while sulfur showed only 3% or less.

A chemical etching technique in conjunction with differential Hall-effect measurements has been used by the authors (24,25) to obtain the first accurate profiles for the implanted layers in gallium-arsenide. In the case of sulfur, a damage-enhanced diffusion has been observed to occur during annealing.

Carbon and sulfur are the only two dopants which could be compared for their electrical activity in low resistivity gallium-arsenide substrates and semi-insulating gallium-arsenide substrates. The

studies on carbon implants by O. J. Marsh et. al. (18) requires further work before any conclusions can be obtained. They have assumed that carbon in doped gallium-arsenide is electrically neutral. Sulfur implants in semi-insulating gallium-arsenide can be considered superior, at least as far as mobility values are concerned. The mobility values in low resistivity substrate implantations were about 1740 cm^2/volt-sec while implants into semi-insulating gallium-arsenide yielded mobility values around 3600 cm^2/volt-sec.

In this thesis the properties of zinc implanted into chromium doped semi-insulating gallium-arsenide are presented. This is the first time that such data are reported. The results are similar to those discussed in the preceding paragraphs for zinc implants into n-type gallium-arsenide. A layer removal technique along with differential Hall-effect and sheet resistivity measurements has been used to obtain an approximate profile for a sample implanted to a dose of $1 \times 10^{15}/cm^2$ and the temperature dependence of resistivity and mobility are also studied. The data to be presented sheds more light on the transport properties of these implanted layers.

CHAPTER III

3. EXPERIMENTAL PROCEDURE

3.1 Hall-Effect and Sheet Resistivity Measurements

Several techniques and sample configurations have been used for the measurement of Hall-effect and sheet resistivity of semiconductor materials (22). Van der Pauw (28) has discussed a method for the combined measurement of Hall-Voltage and resistivity which in principle can be made on a sample of any shape, provided that the sample is homogeneous, uniform in thickness, and small contacts can be made on the periphery of the sample.

The Van der Pauw method can be conveniently used for the Hall-voltage and sheet resistivity measurements of an implanted layer. However, if the electrical measurements are to be representative of the ion implanted layer, the layer should be electrically isolated from the bulk of the substrate. Many people (10, 17, 20) have used a reverse biased p-n junction for such isolation. However, in the present experiments the semi-insulating gallium-arsenide substrate had resistivities of the order of 10^8 ohm-cm and thus acts as an effective electrical isolator.

Figure 3.1. (a) shows the configuration of the sample used. For determining the Hall-voltage a current I_{13} is passed between two opposite contacts and a measurement is made of the voltage change ΔV_{24} occurring between the other two contact pairs when a magnetic induction B is applied normal to the sample surface. The sheet Hall-coefficient R_{HS} is given by

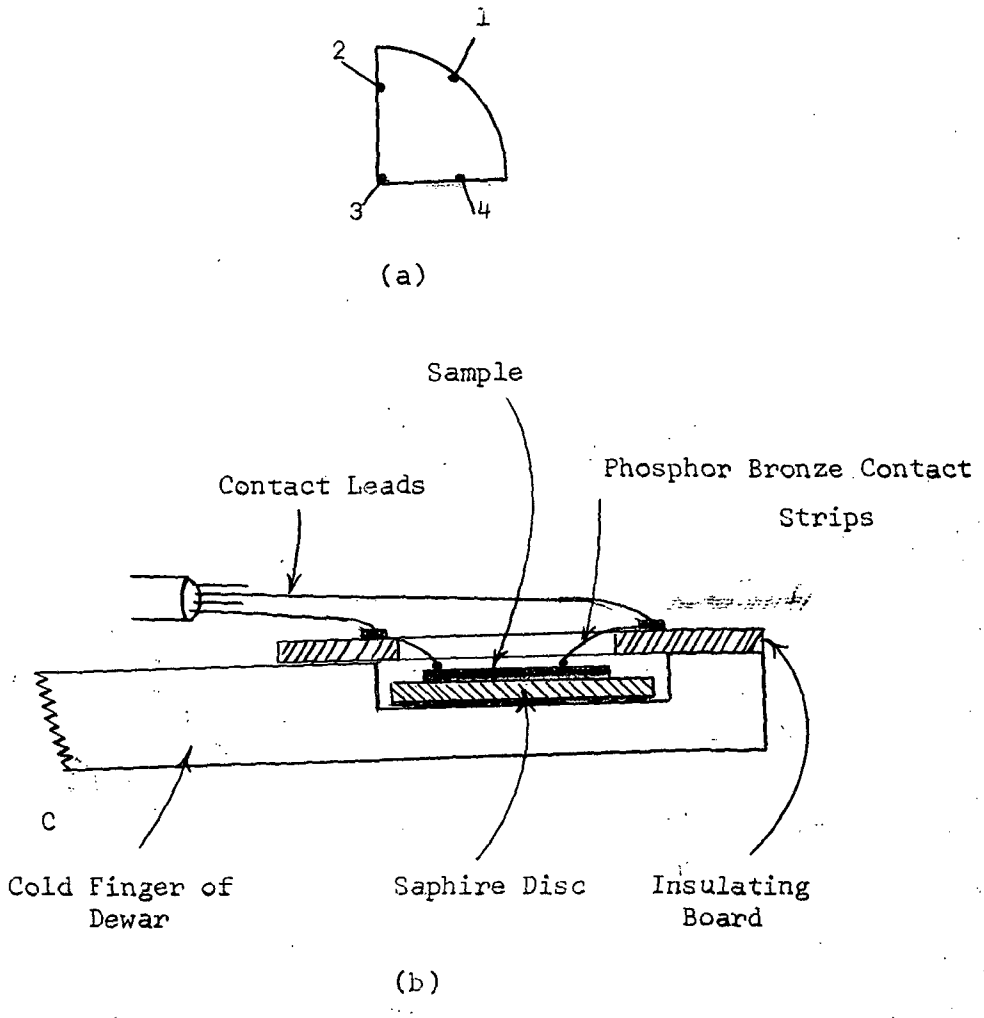

Figure 3.1. Details of sample contacts and sample mounting on cold-finger of the dewar.

$$R_{HS} = 10^8 \times \Delta V_{24}/B \times I_{13} \text{ cm}^2 \text{ coulomb}^{-1} \qquad 3.1$$

where B is in gauss

The sheet resistivity ρ_s is obtained from the potential difference occurring between two adjacent contacts when a current is passed between the other two contacts. For a symmetrical contact pattern the sheet resistivity is given by

$$\rho_s = \frac{\pi}{\ln 2} \frac{V_{34}}{I_{12}} \text{ ohms/square} \qquad 3.2$$

When the pattern is not symmetrical, as in all of the samples used, a geometrical correction factor is required and the sheet resistivity is given by

$$\rho_s = \frac{\pi}{\ln 2} (R_1 + R_2) f(R_1, R_2) \qquad 3.3$$

where $R_1 = V_{34}/I_{12}$; $R_2 = V_{41}/I_{23}$

Here $f(R_1, R_2)$ is the geometrical correction factor. This value was taken from Van der Pauw's paper (28). The spacing of contacts is not critical as the implanted layer depth is always very small compared to the spacing.

The Hall-effect is not the only source of the voltage change observed between the probes. Other galvanomagnetic effects, namely the Nerst, Righi - Leduc, and Ettingshausen effects, can all contribute to the voltage change. If thermal gradients are present they can contribute considerable thermoelectric voltages. In addition , offset voltages will exist between probes. All these effects, except for the Ettingshausen effect, can be eliminated by determining ΔV for the two

polarities of current and magnetic field. The sheet Hall-coefficient is then given by

$$R_{HS_1} = 2{\cdot}5 \times 10^7 \left[\frac{V_{24}(I+, B+)}{V_s(I+,B+)} + \frac{V_{24}(I-,B+)}{V_s(I-,B+)} - \frac{V_{24}(I+,B-)}{V_s(I-,B+)} - \frac{V_{24}(I-, B-)}{V_s(I-,B-)}\right] \times \frac{R_s}{B} \text{ cm}^2 \text{ coulomb}^{-1} \qquad 3{\cdot}4$$

Here B is in gauss and R_s is in ohms, while $V_{24}(I+,B+)$ is the voltage measured between contacts 2 and 4 when the current is passed from contact 1 to contact 3 and a forward magnetic induction is applied. Also $V_{24}(I-, B-)$ is the voltage measured with the current and magnetic field reversed. Similarly $V_{24}(I+, B-)$ is the voltage measured with only the magnetic field reversed, while $V_{24}(I-, B+)$ indicates the voltage measured with the current-direction reversed. R_s is the standard resistance across which the voltage V_s is measured. In a similar manner, R_{HS_2} is calculated from V_{13} the voltage measured between contacts 3 and 1 when the current is flowing between contacts 2 and 4 and the magnetic induction is applied. The Hall-coefficient is then averaged between these readings.

In the same manner the sheet resistivity is also determined by passing the current in two different directions and the sheet resistivity is given by

$$\rho_{s1} = \frac{\pi \times R_s \times f}{4 \ln 2} \left[\frac{V_{34}(I+) + V_{41}(I+)}{V_s(I+)} + \frac{V_{34}(I-) + V_{41}(I-)}{V_s(I-)}\right] \qquad 3{\cdot}5$$

V_s is measured across the standard resistance R_s. Again f is the

geometrical correction factor obtained as explained above. In a similar manner ρ_{s2} is calculated and the sheet resistivity is taken as the average of these two results. If the conductivity mobility is assumed to be equal to the Hall-mobility then the surface carrier concentration (n_s) can be calculated from a measurement of ρ_s and μ_H. The following formulae are used.

$$\mu_H = \frac{R_{Hs}}{\rho_s} \text{ cm}^2/\text{volt-sec and } n_s = \frac{1}{e\mu_H\rho_s} / \text{cm}^2 \qquad 3.6$$

The value of e, the charge of an electron, is $1{\cdot}6 \times 10^{-19}$ coulombs. The thermoelectric power is assumed to be negligible. It is also assumed that the implanted layer is isotropic. However, not all transport properties need be isotropic. One example is the magneto-resistance. This was calculated and found to be negligible.

The Hall-effect and resistivity measurements were taken in vacuum in a cryostat system similar to that described by Johansson and Mayer (12). To minimize the leakage current all leads were enclosed in individual teflon tubing and shielded by copper braided tubing. Noise pick up, which was a severe problem due to the high resistance of the sample, was reduced by floating the system and by having the system ground only at the electrometer. The insulation resistance of the system at various stages was checked from time to time and was kept well above 10^{11} ohm. The sample was always covered in the dewar so that no spurious reading was obtained by stray incident light. Small copper spheres soldered to phosphor bronze strips were plated with a gold - 0.5% zinc plating solution. This was riveted to a circuit board and the phosphor bronze strips were used as pressure contacts.

This provided a satisfactory ohmic contact even to high resistivity layers. Each time a sample was mounted the contacts were checked for ohmicity by a curve tracer.

The sample was always cleaned in deionized water for a minimum of five minutes to ensure a clean surface. Trichoroethylene and methanol baths preceded this. The sample was fixed to a saphire disc with Apeizon wax. The details of the sample mounting to the dewar cold finger is given in Figure 3.1(b). Figure 3.2 gives the details of the electrical connections. A Keithley model 625 constant current source was used along with a Keithley model 225 nanovolt - d.c. amplifier and a Doric integrating digital voltmeter as a read out device. When the sample resistance exceeded the input impedence level of the nanovoltmeter a Keithley 602 electrometer was used as the voltage measuring device followed by the digital voltmeter.

To ensure the reliability of the system a p- type gallium-arsenide sample whose specifications are given by the manufacturer was measured and the results are shown in table 3.1. The linearity of the Hall-effect was checked by varying the field up to 16 kilogauss for various current values. The result is shown in Figure 3.3.

During the low temperature measurements the dewar was evacuated by a diffusion pumped vacuum system to pressures about 5×10^{-5} torr. A proportional temperature controller was used to maintain the temperature at any intermediate value between liquid nitrogen and room temperature. Four half watt 40 ohm resistors were used to heat the cold finger. The sample, cold finger, and the heating resistors were all in good thermal contact. Heat radiation from the sample was reduced by wrapping the entire sample with a brass strip in contact

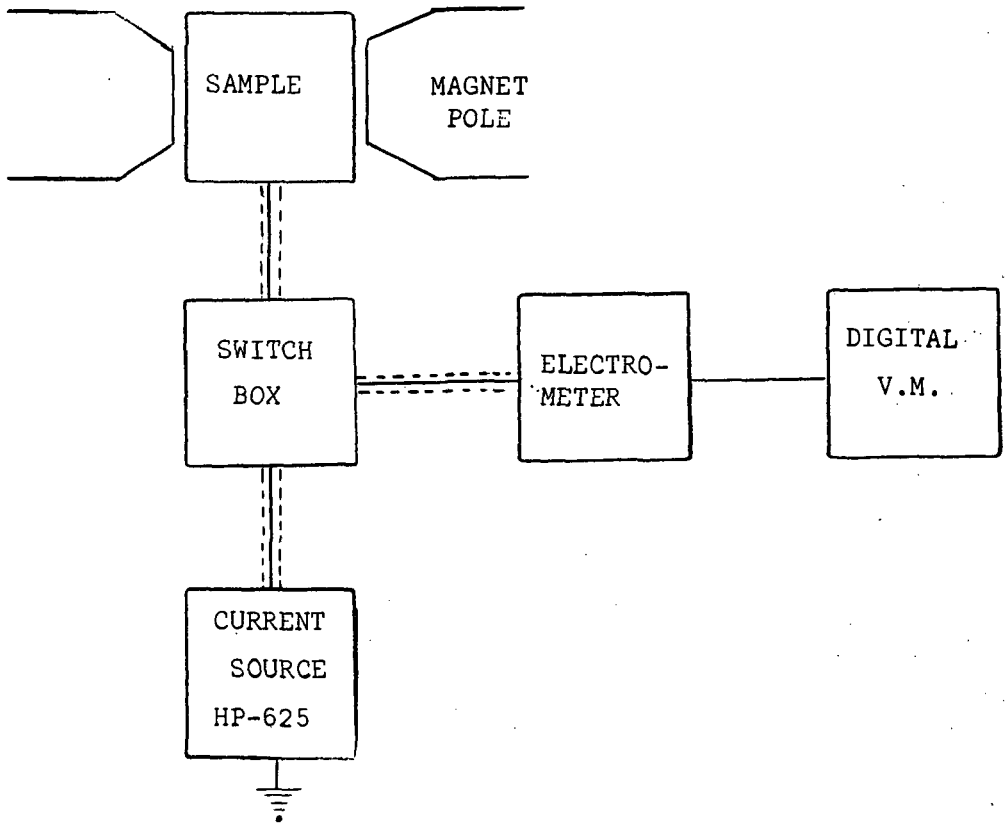

Figure 3.2. Schematic diagram of the measurement circuit.

TABLE 3.1. Comparison of the measured and specified values of a standard sample.

Property	Measured Values	Manufacturer's Specification
Resistivity	0.209 ohm-cm	0.34 - 0.19 ohm-cm
Mobility	261 cm^2/volt-sec	266-240 cm^2/volt-sec
Carrier-Concentrations	$1 \cdot 145 \times 10^{17}/cm^3$	$9 \times 10^{16} \sim 1 \cdot 4 \times 10/cm^3$

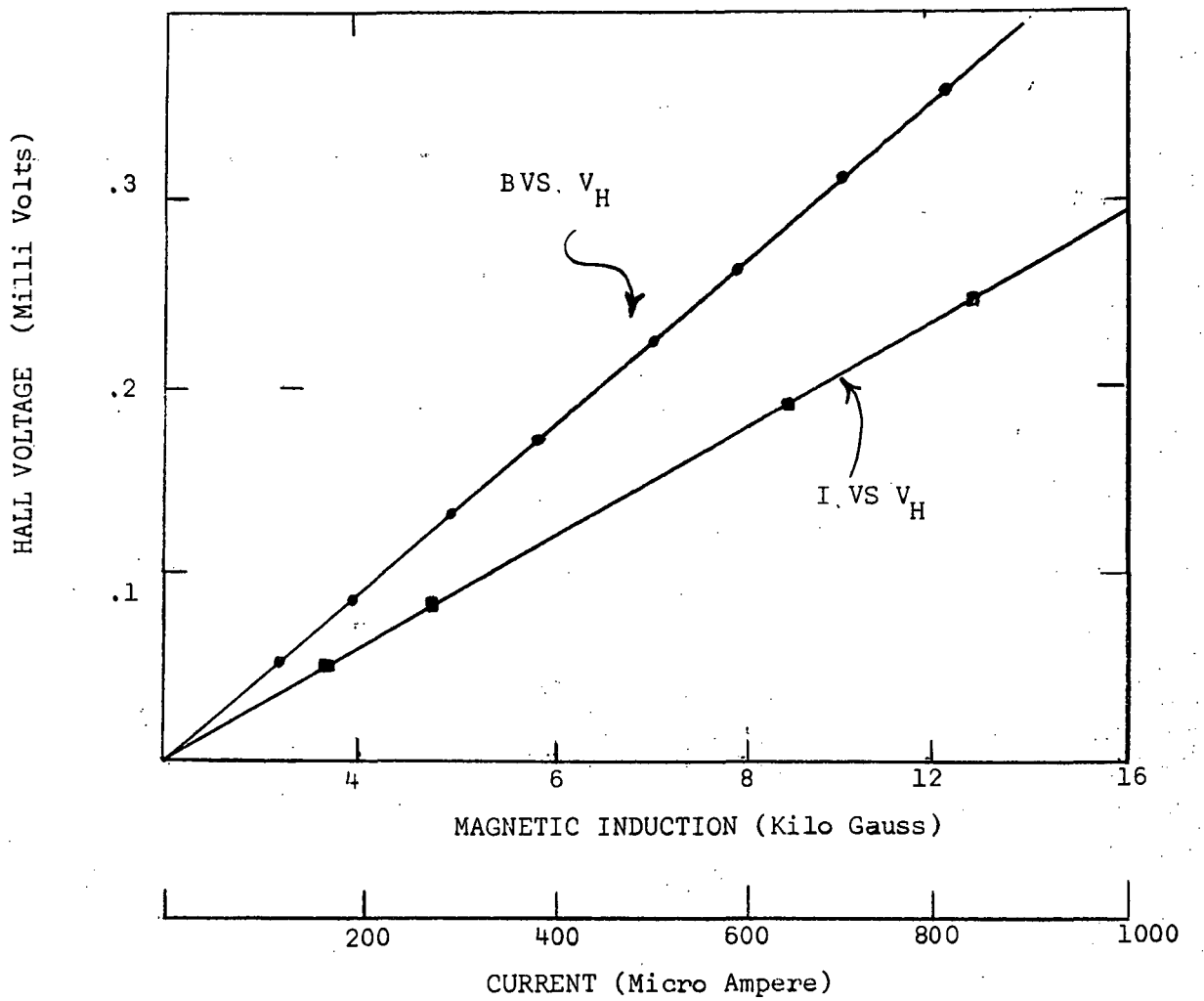

Figure 3.3. Graph showing the linearity of the Hall-effect measurements on a standard sample.

with the cold finger. Temperature stability was normally obtained within ten minutes. However, twenty minutes were allowed between two temperature settings.

3.2 Sample Implantation and Annealing

The samples were prepared from commercially available <111> oriented gallium-arsenide wafers approximately 20 mils thick. The samples were high resistivity semi-insulating gallium-arsenide compensated by chromium doping. The ion implantation has been performed in NASA Langley Research Center Laboratories using a magnetically separated beam at 60 KeV. The substrate has been kept at room temperature during implantation. The implantation was done in a random direction, and no special care was taken to orient the sample with respect to the ion beam. Small samples were diced from the large implanted wafers and used for measurements. The samples were annealed inside a quartz tube with nitrogen flow for a period of 30 minutes in all cases.

The two major problems associated with the annealing of ion implanted gallium-arsenide are out-diffusion of the implanted zinc and the decomposition of the gallium-arsenide above 650°C. The outdiffusing of zinc was indicated by the fact that the implanted depth is shallow, less than 1000Å, and zinc has a high diffusion coefficient in gallium-arsenide. Hunsperger et. al. (8, 10) have suggested covering the implanted sample with another gallium-arsenide sample as a simple alternative to the usual arsenic charged ampoule method of annealing. The same group of authors (18) have pointed out to support the out-diffusion theory, that the cover gallium-arsenide

wafer did become p- type, even though they were not implanted. In this case the use of a cover gallium-arsenide wafer as the only means of protection is questionable at elevated temperatures above 600°C.

A more reliable surface protection has been used by the same authors (17) by having a thin film of silicon-dioxide (SiO_2) deposited over the implanted region. This serves the purpose of a diffusion barrier (18). The silicon-dioxide film can be obtained either by sputter deposition or by chemical reaction of tetraethyl-ortho-silicate. These are time consuming processes.

In the present experiments, a new coating technique was used in which the silicon-dioxide film was obtained using a photo-resist type spinner. The coating material is a low viscosity alcoholic solution (manufactured by Emulsitone. Co., Livingston, N. J.) which forms hydrous silicon dioxide when applied in air. This layer was baked at 200°C for 10 minutes and during the earlier part of the experiments the baking was done in air. Later it was done under a low vacuum of 10^{-1} torr. The silicon-dioxide layer was obtained by spinning the sample at 4000 RPM for 20 sec. A film of approximately 2000 Å was obtained. However, a few samples had to be discarded after 800°C annealing because the film separated from the gallium-arsenide and formed small bubbles under which decomposition occurred.

A sample implanted to a dose of $3 \times 10^{13}/cm^2$ was annealed in steps of 100°C up to 800°C. At each stage the sample was protected by sandwiching between two unimplanted semi-insulating gallium-arsenide wafers. At high temperatures, the partial pressure of arsenic from

the wafer above and below is expected to give protection to the implanted sample. The mobility at different annealing temperatures of this sample is compared with the standard SiO_2 protected sample having the same implantation dose in Figure 3.4. It is evident that the sandwiching technique does not prevent decomposition above 500°C. All the subsequent samples were protected only by SiO_2 layers.

3.3 Layer Removal Measurements

The interpretation of Hall-effect and resistivity measurements on implanted samples is influenced by the fact that both carrier concentration and mobility are depth dependent. The values obtained by using equation 3.6 are only weighted averages. When both the carrier concentration and the mobility are functions of depth, differential measurement with thin layer removal is required. As derived and explained in Appendix - 1, the mobility and carrier concentration at a perpendicular distance x from the surface is given by

$$\mu_h(x) = \frac{d(R_{HS}\sigma_s^2)}{dn} \quad \frac{d\sigma_s}{dx} \qquad 3.7$$

$$n(x) = \frac{\mu_h(x)}{e\,\mu_c(x)} \quad \left(\frac{d\sigma_s}{dn}\right)^2 \Big/ \quad \frac{d\,(R_{HS}\sigma_s)}{dp} \qquad 3.8$$

These assume accurate measurement of the thickness removed. Several methods of removing a thin layer were tried. They include chemical etching and anodic stripping. In all cases either the etch rate was too rapid or there was preferential etching of A or B face of the single crystal. J. D. Sansbury and J. F. Gibbons (25) have successfully used an etchant consisting of H_2SO_4 : H_2O_2 : H_2O in the ratio of 1 : 1 : 100 and have reported an etch rate of 300 ∿ 450 Å per

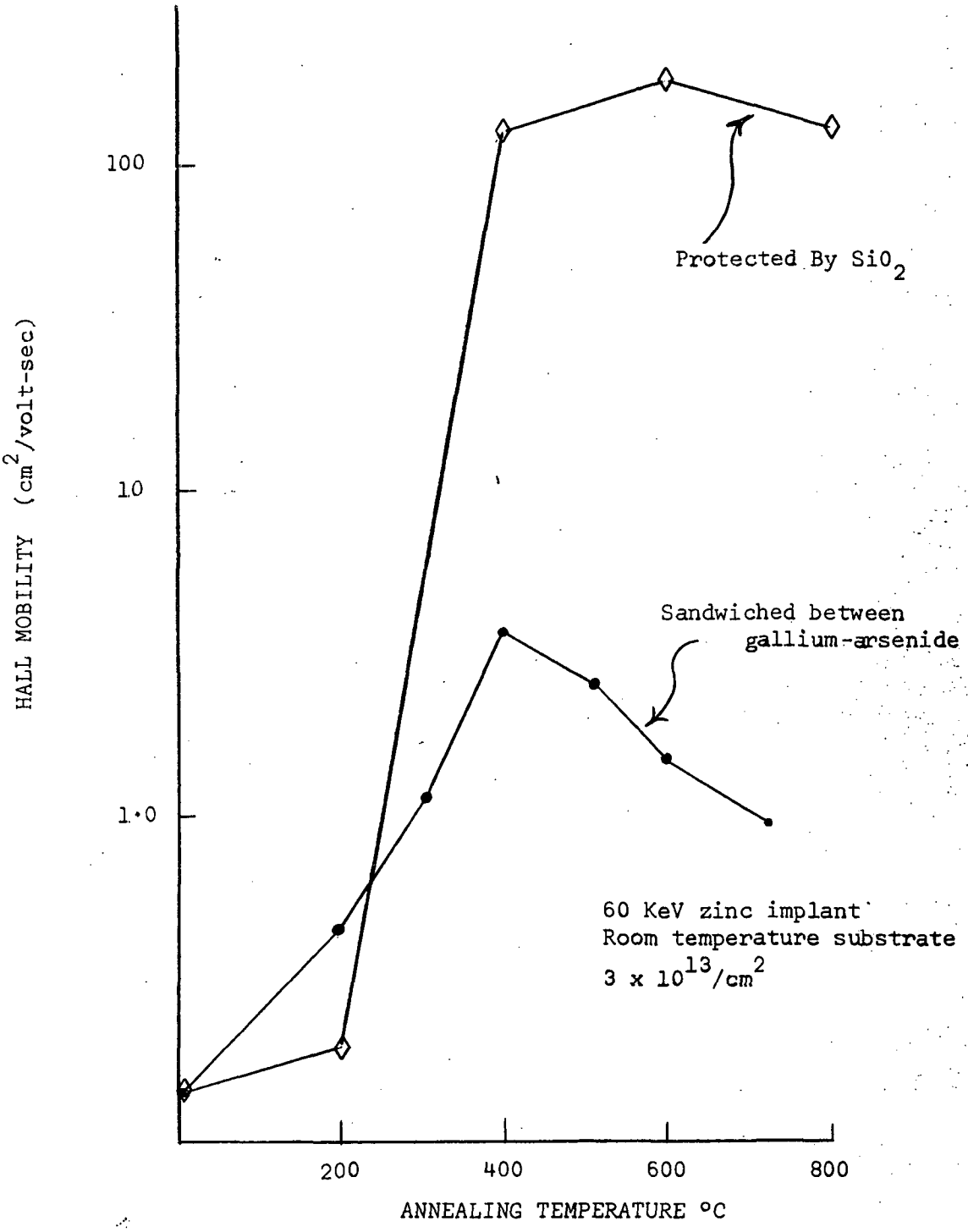

Figure 3.4. Mobility value comparison at different annealing temperatures for a sandwiched and SiO_2 protected sample.

Figure 3.4. Mobility value comparison at different annealing temperatures for a sandwiched and SiO_2 protected sample.

minute. The etchant does not deteriorate for several hours. In the present experiments an etchant of the same composition was used and the thickness of layer removed was calculated under the assumption of an etch rate of 400 Å per minute. After each etching, the sample was cleaned in deionized water for at least five minutes, dried, and then Hall-effect and sheet resistivity measurements were made.

The results obtained by these measurements are presented in subsequent graphs and the conclusions drawn are discussed in the next chapter.

CHAPTER IV

4. RESULTS AND DISCUSSIONS

The results of various experiments are given in the form of eight graphs in this section. The conclusions that could be drawn from them are discussed and summarized.

Six different doses of $1 \times 10^{12}/cm^2$, $1 \times 10^{13}/cm^2$, $3 \times 10^{13}/cm^2$, $1 \times 10^{14}/cm^2$, $3 \times 10^{14}/cm^2$ and $1 \times 10^{15}/cm^2$ zinc ions were implanted at 60 KeV at room temperature. Each of these samples were annealed in a nitrogen atmosphere at 200°C, 400°C, 600°C and 800°C for 30 minutes. After each annealing the sheet resistivity and Hall-effect measurements were made by the Van der Pauw method. The sheet resistivity dependence on temperature, from liquid nitrogen temperature to room temperature after each annealing, was measured on a $1 \times 10^{14}/cm^2$ sample. After chemically etching thin layers from a $1 \times 10^{15}/cm^2$ sample, sheet resistivity and Hall effect measurements were made. These data were used to obtain the mobility and net carrier concentration profile of the $1 \times 10^{15}/cm^2$ implantation.

The results are in the subsequent sections.

4.1 Effective Surface Concentration Behavior

The effective surface concentration in each case was determined using the sheet resistivity and Hall-mobility values, assuming that the Hall and conductivity mobilities are equal. Figure 4.1. shows the effective surface concentration as a function of the annealing temperature for each implantation dose. The same data is replotted in Figure 4.2. to represent the implanted concentration and the final active concentration after each annealing. It is observed that up to

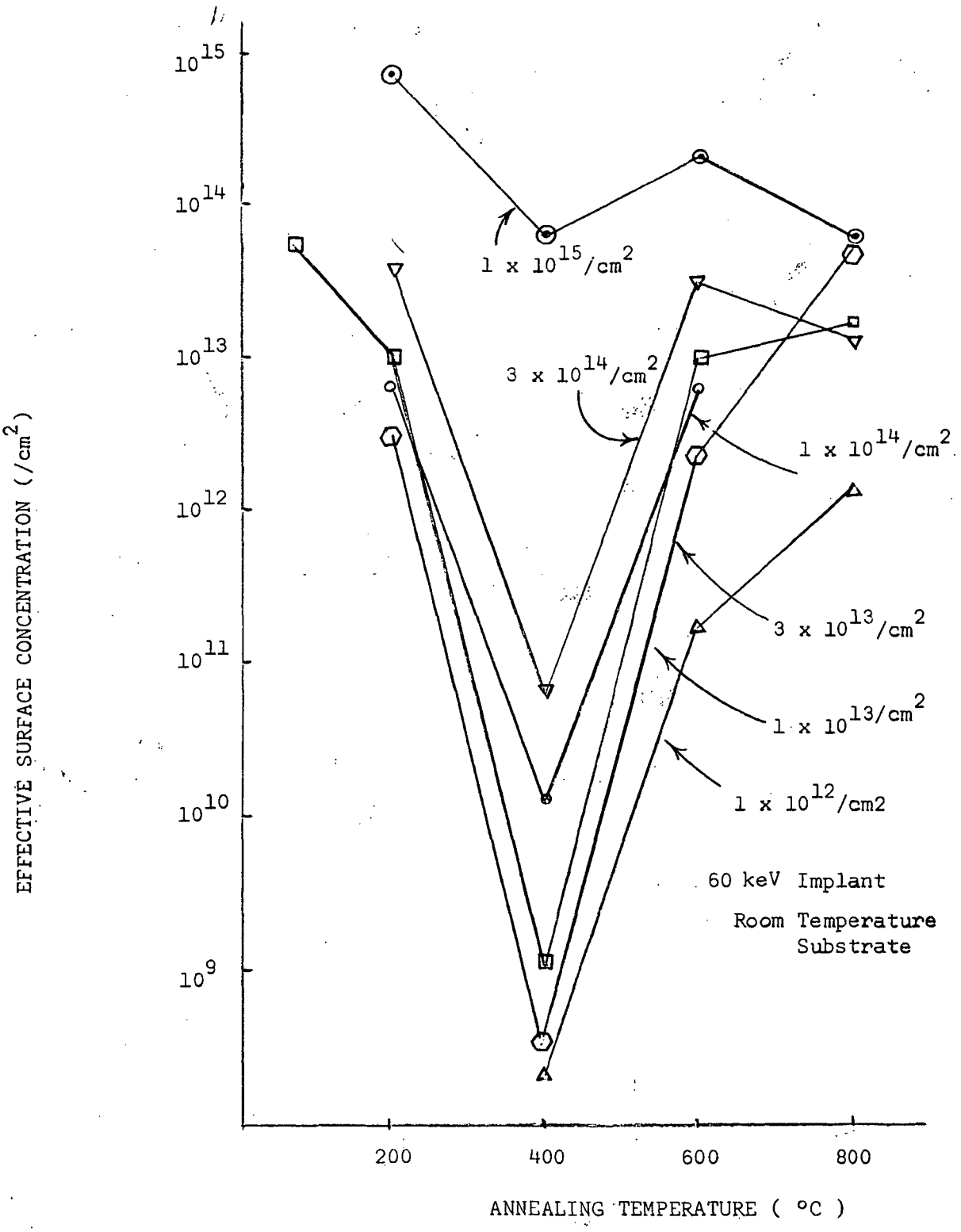

Figure 4.1. Implantation dose dependence of effective surface concentration versus annealing temperature.

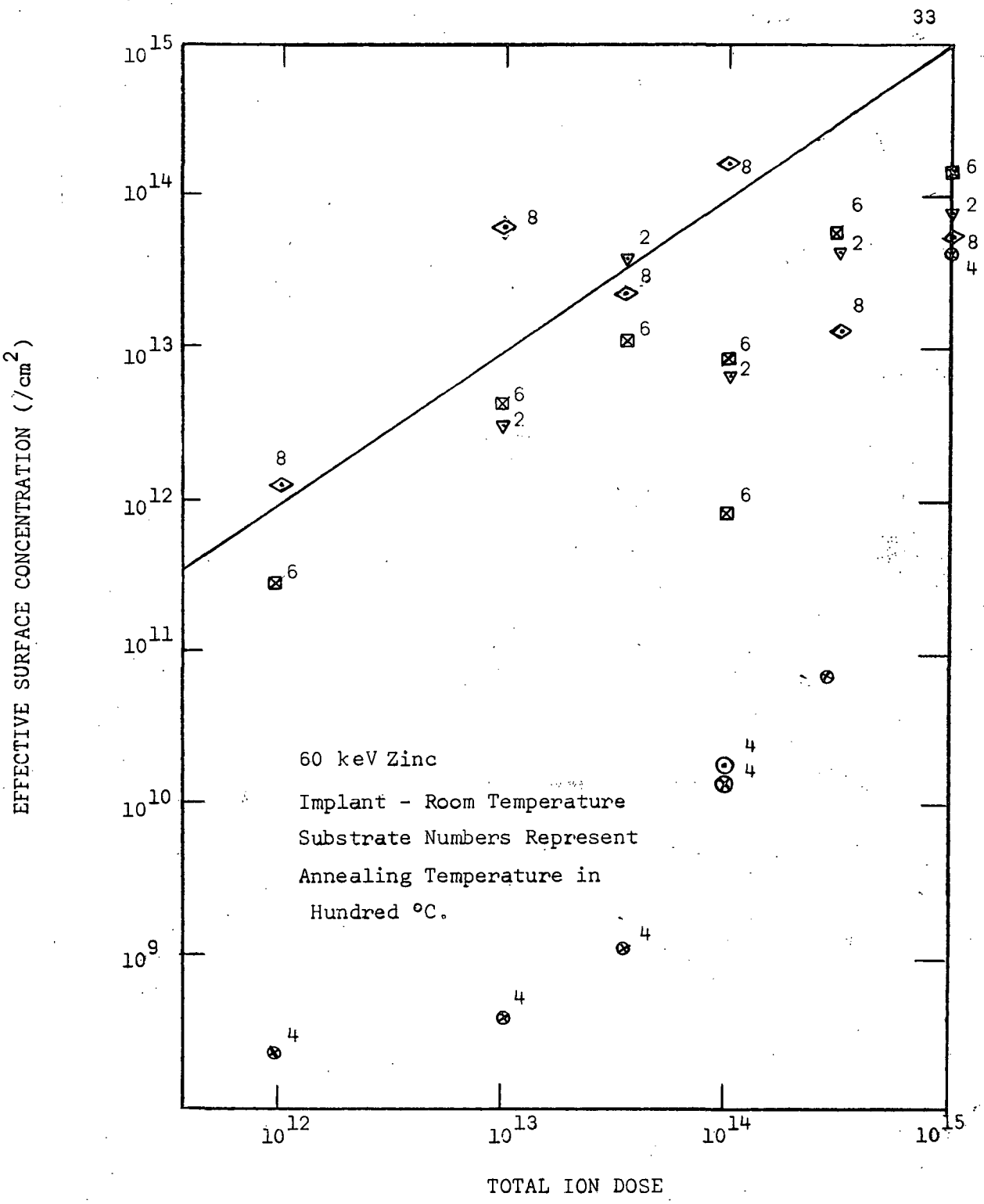

Figure 4.2. The implantated dose and the effective surface concentration at different annealing temperatures.

a dose of $10^{14}/cm^2$ there is nearly a 1:1 correspondence of the active ions and the implanted dose. Above this dose, the effective surface concentration after 800°C annealing saturates around $5 \times 10^{13}/cm^2$ and is nearly independent of the implantation dose. Similar saturating effects in low-resistivity gallium-arsenide have been observed by Marsh et. al. (17) for cadmium implantations.

Several possible explanations have been given to justify the low activity at high implantation doses. Insufficient annealing time could be one possible reason. In the present case all samples have been annealed for 30 minutes. Marsh et. al. (18) have given the annealing characteristics of zinc implanted diodes in low resistivity gallium-arsenide and have shown that most of the annealing occurred in the first six minutes and that the subsequent 30 minutes of annealing had little effect. Based on the above results, it is expected that annealing will be complete in 30 minutes. However, this was not experimentally confirmed for the present implantations in semi-insulating gallium arsenide.

In many cases, the saturation effect is attributed to the solid solubility limit of the impurity in the given substrate (12). The solubility limit of zinc in gallium-arsenide at 800°C is $1.6 \times 10^{20}/cm^3$ as given by Chang (5). Considering a $3 \times 10^{14}/cm^2$ implant and assuming that the maximum concentration reached is limited by the solid solubility, the corresponding range straggling is calculated to be 41Å. For a 60 KeV zinc implant into gallium-arsenide, the range straggling is around 114Å (14). The minimum range straggling is about half of the theoretical value. From this we cannot conclusively conclude that the saturation effect is not due to the solid solubility. The actual range

and straggling were not measured.

Baron et. al. (1) have suggested that, due to the dissociation of radiation damage complexes, compensating centers could be formed. The nature of these complexes are not known. These authors have suggested a model in which the defect centers act as acceptors compensating the bismuth implanted in silicon (1). Sansbury et. al., (25) have reported such radiation defect centers and their enhanced diffusion during subsequent annealing for sulfur implanted in gallium-arsenide. It is believed that in the present case the low effective concentration of zinc at high doses is caused by defect centers. These defect centers could be either donors or acceptor type complexes. This will be discussed in more detail in Section 4.3.

4.2 Hall Mobility Behavior

The Hall-mobility is directly related to the magnitude of the Hall-voltage and the resistivity of the sample. The mobility of the unannealed sample could vary be a factor of two due to the very low Hall-voltage. Similarly, the values after the 400°C anneal could have about 50% error for doses less than $10^{14}/cm^2$ due to the noise of the system at resistivities above 10^8 ohms per square.

In Figure 4.3. the recovery of mobility with annealing temperature is noted. There was a large increase up to 400°C and the mobility saturated for 600°C and 800°C annealing except for the $10^{12}/cm^2$ dose. After 800°C annealing typical mobilities of about 50 $cm^2/volt^{-1}\ sec^{-1}$ to 125 $cm^2/volt^{-1}\ sec^{-1}$ were attained. The only published values of mobility in semi-insulating gallium-arsenide are those of Hunsperger

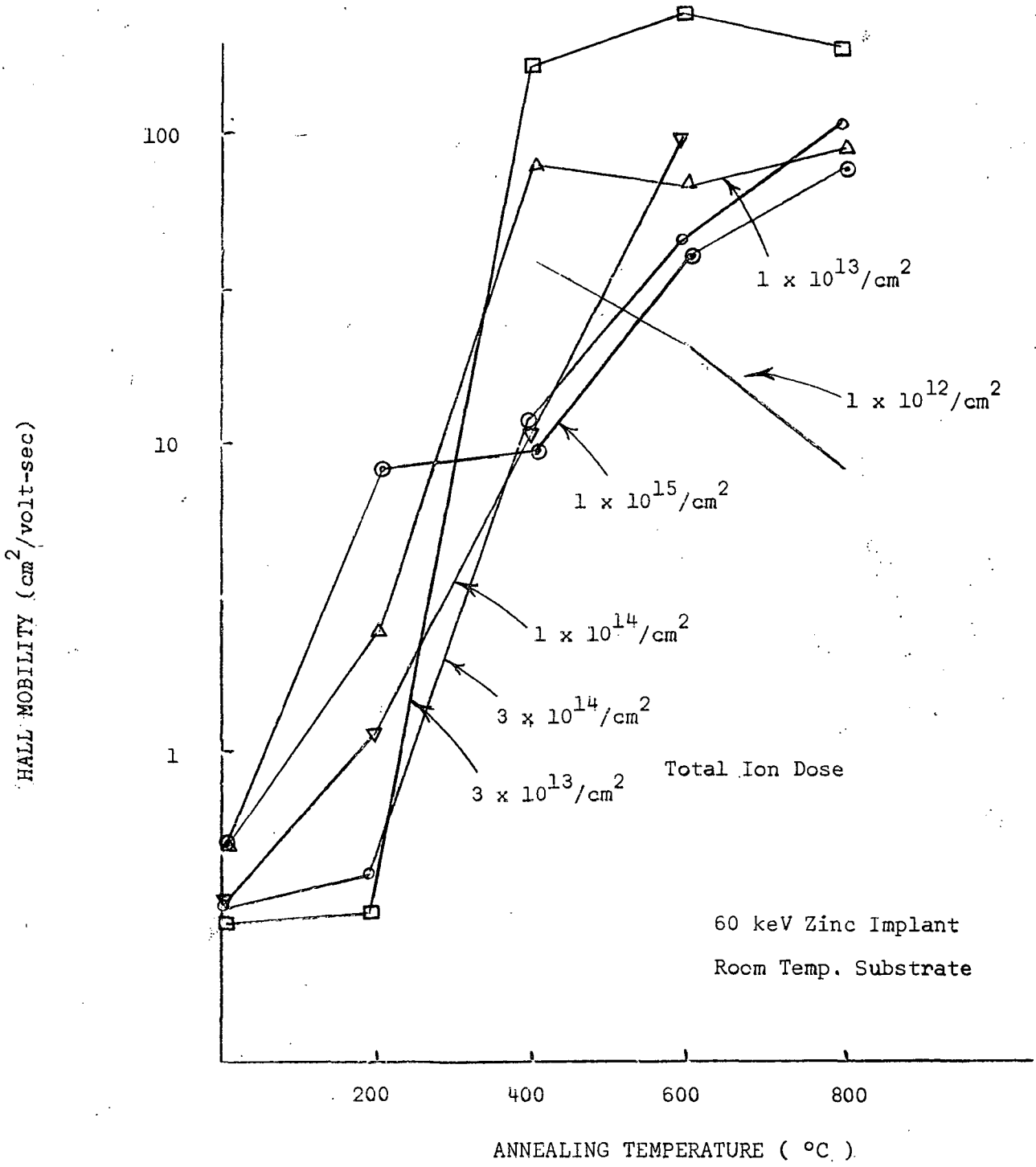

Figure 4.3. Hall mobility dependence at different annealing temperatures for various implantation dose.

et. al. (12) for a room temperature zinc implantation at 20 KeV. These workers report that the data points were scattered and no reading was possible up to 300°C annealing. However, for a $1 \times 10^{16}/cm^2$ dose, a mobility of 20 cm^2 $volt^{-1}$ sec^{-1} is reported after 600°C annealing. There is only one case (11) where after 900°C a mobility of 100-125 cm^2 $volt^{-1}$ sec^{-1} is reported.

The mobility values for a $10^{12}/cm^2$ dose decreased with annealing temperature. Moreover, contrary to the expected high mobility due to the smaller doping level, the maximum mobility of only 25 cm^2 $volt^{-1}$ sec^{-1} was obtained after 400°C annealing. From the sheet resistivity behavior it is concluded that the implantation dose level should be at least $1 \times 10^{13}/cm^2$ to overcome the influence of the chromium atoms in the substrate. The very low mobility for the $10^{12}/cm^2$ dose strengthens the conclusion that the chromium atoms of the substrate influences the properties below a dose of $10^{13}/cm^2$ and this restricts attaining carrier concentrations below 1×10^{17} cm^{-3} in semi-insulating gallium-arsenide by ion implantation.

The mobilities are shown as a function of the final measured surface carrier concentration in Figure 4.4. Sze and Irvin's (27) experimental data is given, along with a theoretical curve which assumes that ionized impurity scattering and lattice scattering are the only mechanisms affecting mobility. The ionized impurity scattering is assumed to follow the Brook-Herring relation (2). A lattice mobility of 450 $cm^2v^{-1}sec^{-1}$ is assumed following Rosi et. al. (23). It is also assumed that the implanted layer is uniformly

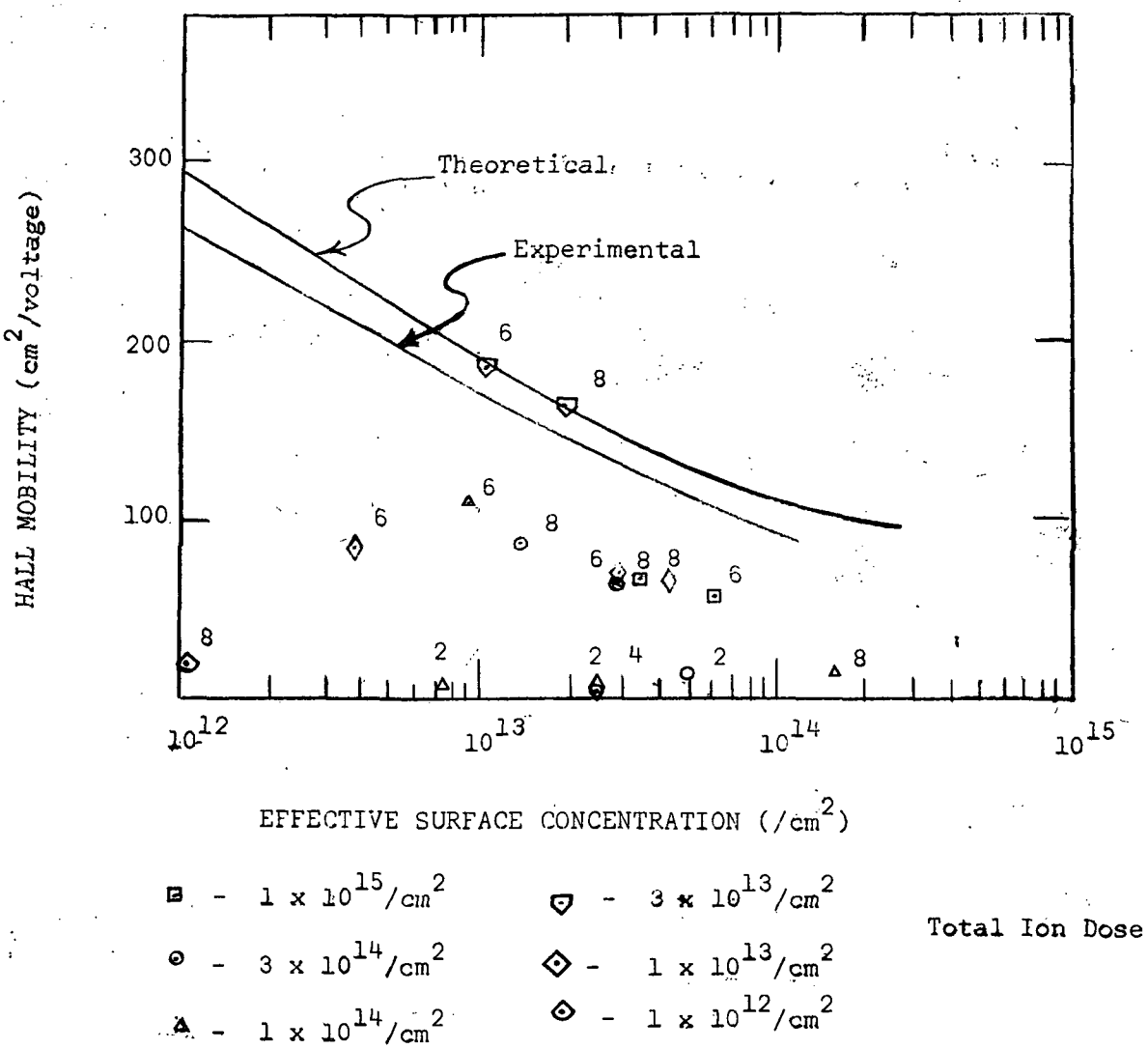

Note: Numbers adjacent to data points denote annealing temperature in hundreds of °C for 30 minute period.

Figure 4.4. Theoretical and experimental values of Hall mobility at different effective surface concentrations.

distributed over 1000 Å to allow the plotting of the theoretical graph as a function of the surface concentration. The depth of the implanted layer as measured by the layer removal technique supports this assumption of 1000Å.

The data indicate that the mobility in the ion implanted layer decreases as the carrier concentration increases, which is typical of ionized impurity scattering. However, the mobility for 200°C and 400°C are much lower than the theoretical value.

The temperature dependence of mobility and resistivity for a $1 \times 10^{15}/cm^2$ dose sample from liquid nitrogen temperature to room temperature is shown in Figure 4.5. It is clearly seen that the mobility decreases with temperature at low temperatures and supports the conclusion that the mobility is dominated by an ionized impurity scattering mechanism. The resistivity decreased with increasing temperature.

4.3 Effective Sheet Resistivity Behavior

The room temperature sheet resistivity annealing characteristics are presented in Figure 4.6. The sheet resistivity was measured as a function of temperature for a $1 \times 10^{14}/cm^2$ sample and the results are given in Figure 4.7.

In the as implanted condition the sheet resistivity was independent of dose. Sansbury et. al. (25) have observed similar sheet resistivities of almost equal magnitude in the as implanted condition for different doses of silicon implanted at 50 KeV in semi-insulating gallium-arsenide. The $1 \times 10^{12}/cm^2$ sample had higher sheet resistivity. In this case probably the effect of the initial lattice damage is not enough to overcome the compensating effect of the chromium-doped sub-

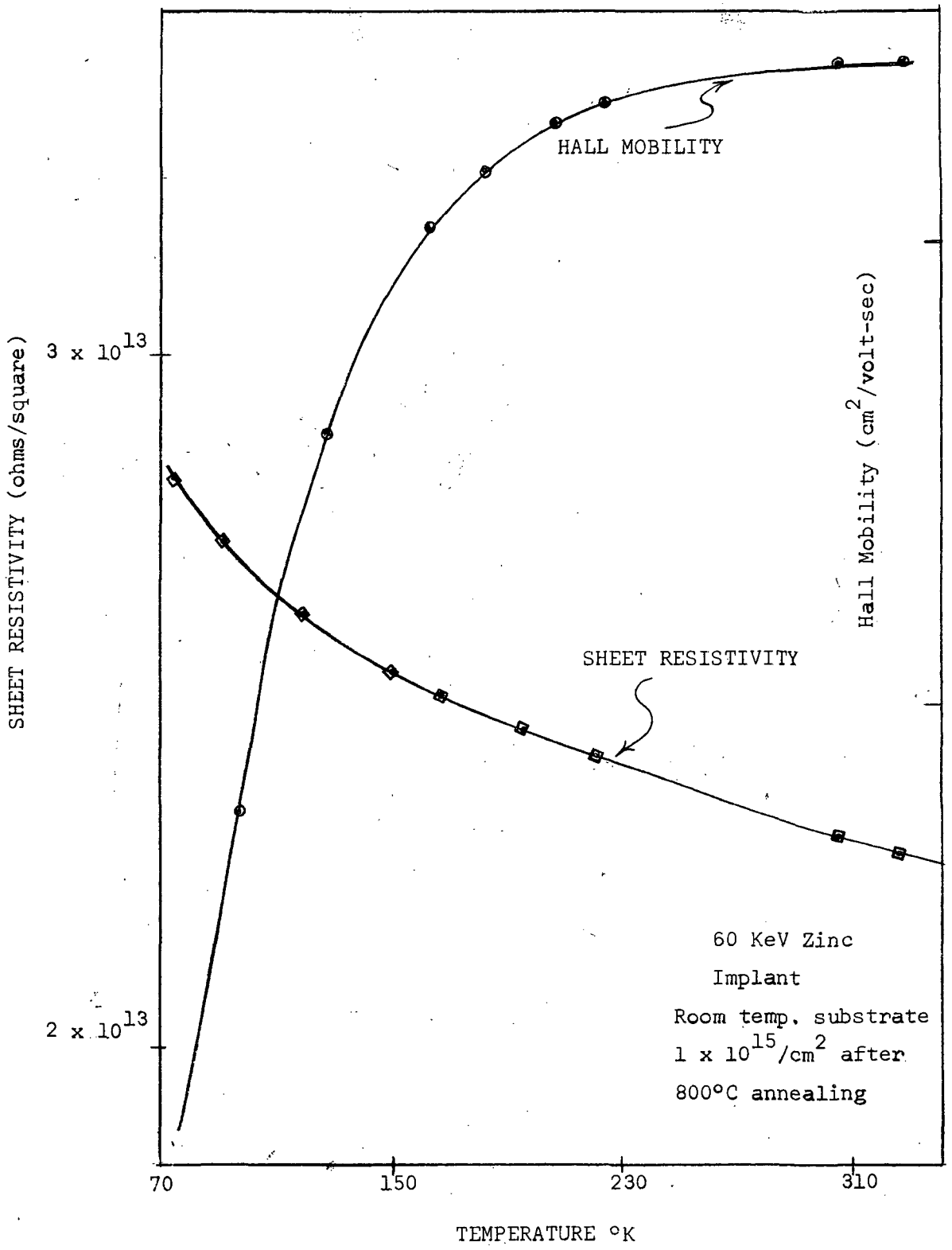

Figure 4.5. Temperature dependence of effective resistivity and mobility after 800°C for an implantation dose of $1 \times 10^{15}/cm^2$.

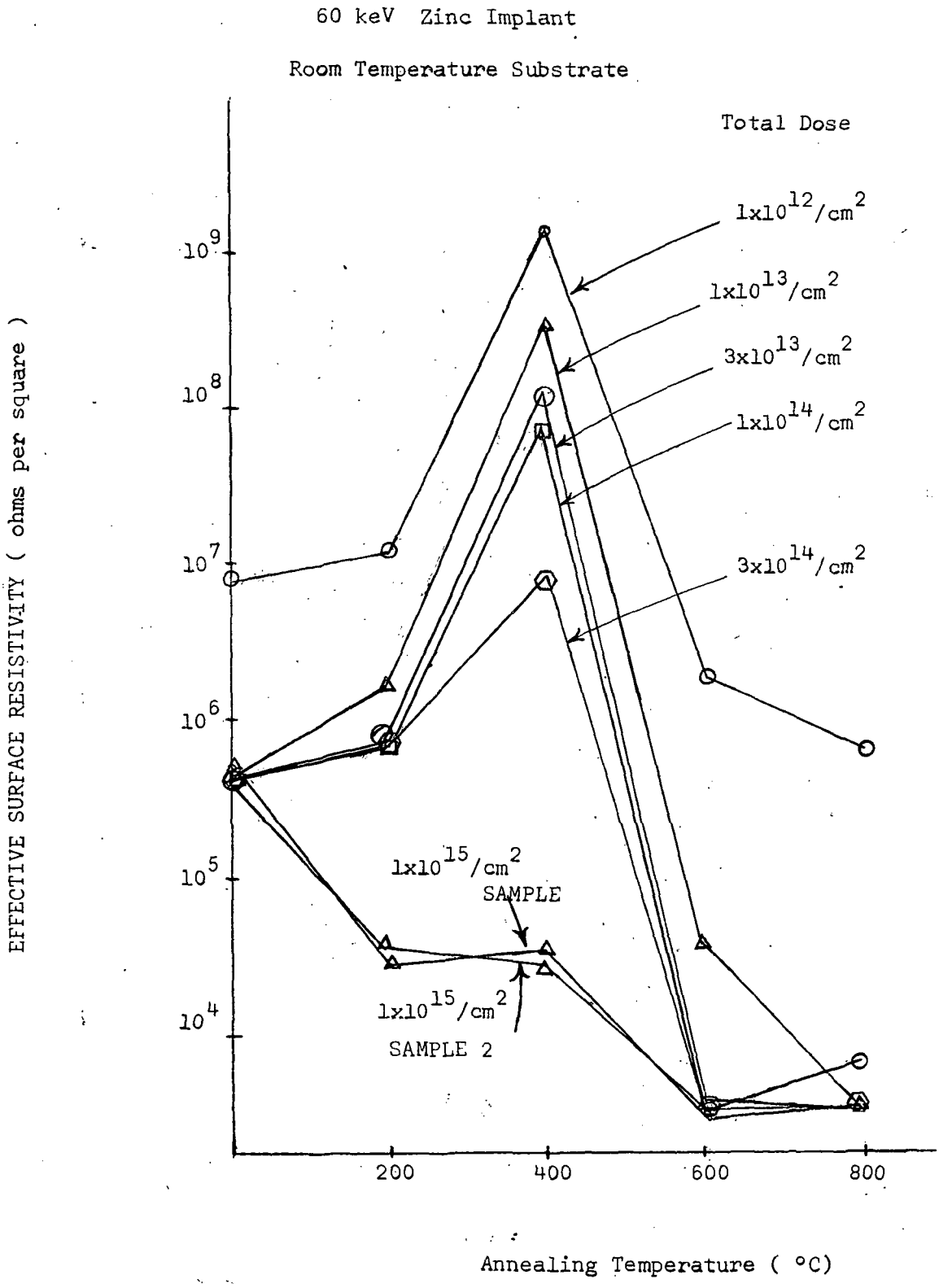

Figure 4.6. Effective surface resistivity values for different implantation dose at different annealing temperatures.

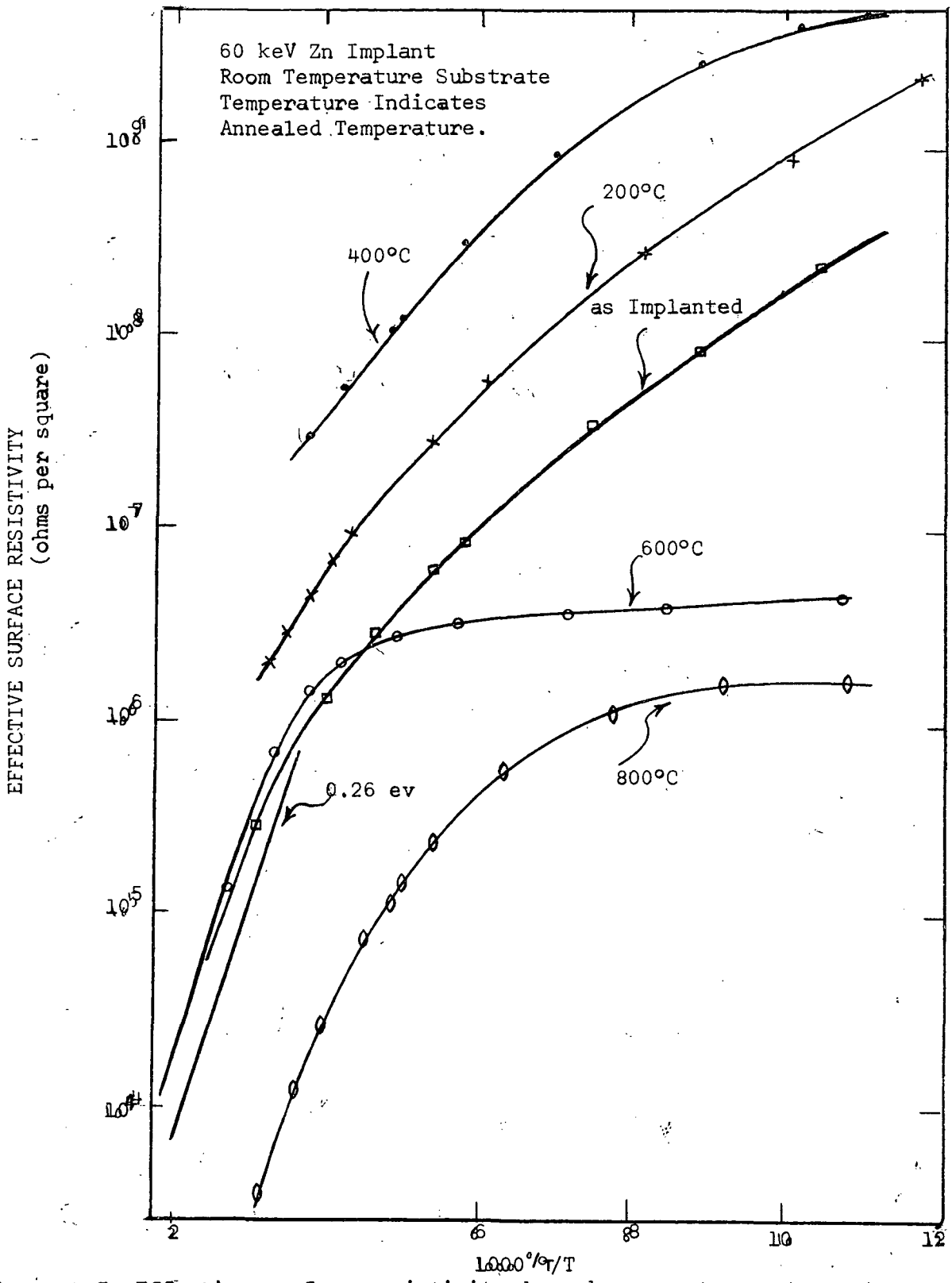

Figure 4.7. Effective surface resistivity dependence on temperature at different annealing temperatures for an implanted dose of 1×10^{14} /cm^2

strate.

The sheet resistivity increased up to 400°C, with annealing, and then began decreasing rapidly for all doses below 3 x $10^{14}/cm^2$. For a dose of 1 x $10^{15}/cm^2$ the sheet resistivity decreased steadily. Hunsperger et. al. (11) have reported the same kind of behavior for a 20 KeV room temperature zinc implant. Their results are reproduced in Figure 2.2. It is seen there that for a dose of 1 x $10^{16}/cm^2$ the sheet resistivity steadily decreases with annealing temperature and for the rest of the doses there is first an increase in the resistivity and then a decrease. The results of Sansbury et. al. (25) for the silicon implant in semi-insulating gallium-arsenide are of the same nature as in Figure 4.6. The maximum sheet resistivity occurred around 400°C. One sample with a 1 x $10^{13}/cm^2$ dose was annealed at 400°C and 500°C. The sheet resistivity was lower after 500°C annealing by a factor seven compared to the value at 400°C. Sansbury et. al., (24) have reported the maximum sheet resistivity occurring at 500°C for one sample and 400°C for another sample of gallium-arsenide implanted with silicon.

For the annealing temperatures above 400°C there was a steady decrease in sheet resistivity. The final sheet resistivity was between 5 x 10^3 - 1 x 10^4 ohms per square. The sheet resistivity after 800°C was independent of dose, except for the sample with a 1 x $10^{12}/cm^2$ dose which showed a considerably higher resistivity of 4.6 x 10^5 ohms per sq. It is believed that the electrical activity of the implanted ions is not sufficient to overcome the substrate doping properties and hence the high sheet resistivity. Assuming the chromium doping to

have a concentration of $5 \times 10^{16}/cm^3$, as assumed by Sansbury et. al., (24) and 100% activity of the implanted $10^{12}/cm^2$ dose to a depth of 1000 Å, gives an estimated surface resistivity of 6.1×10^5 ohms per square. This calculation assumes a mobility of 20 cm^2 $volt^{-1}$ sec^{-1}. This number is close to the measured value and indicates that the substrate chromium doping plays a major role in limiting the lower bound of the implantation dose. The implantation should at least produce $5 \times 10^{17} - 1 \times 10^{18}$ active ions/cm^3 to have electrical properties independent of the substrate. This could easily be achieved by a $1 \times 10^{13}/cm^2$ ion dose implantation.

In attempting to give a possible explanation of the sheet resistivity behavior with annealing temperature two models could be considered. The initial increase of resistivity up to 400°C and then an abrupt decrease at 600°C annealing are to be explained.

Mayer et. al. (19) and Baron et. al. (1) have discussed a two layer model with carrier concentrations and mobilities of N_1/cm^3, μ_1, cm^2 $volt^{-1}$ sec^{-1} and N_2/cm^3, μ_2 cm^2 $volt^{-1}$ sec^{-1}, on the usually-measured effective sheet resistivity and effective Hall-mobility. These measured quantities are weighted averages. The authors (19,1) have shown that these weighted averages depend on the μ_1/μ_2 and N_1/N_2 ratios and are representative of the layer having higher concentration or mobility. In the same manner, in all of these ion implanted samples one can assume a heavily damaged first layer and a second layer of less damage. The second layer could be a channelled tail. For annealing up to 400°C, the first amorphous layer has less influence on the electrical properties because of its low mobility.

The tail anneals first and the properties measured are mostly influenced by the tail distribution. Since the concentration in the tail is so low, higher resistivities result. Above 400°C annealing, the first layer reorders and the zinc ions become active. Since the N_1/N_2 ratio is high above 400°C the properties measured are influenced by this first layer where most of the implanted ions reside. This gives a satisfactory explanation for the sheet resistivity behavior. However, when attempting to explain the lower number of active impurities for higher dose, as seen earlier, this model fails to give a reason.

There is another possible explanation. The nature of the radiation damage and the effect of subsequent annealing on it is quite complex. From the temperature dependence of resistivity the existence of deep lying defect centers is postulated. These could be acceptor type vacancy complexes or donor type compensating centers. This model using defect centers could explain the resulting low activity of the implanted atoms. A measurement of the temperature dependence of the resistivity will reveal the presence of the defect centers and their activation energy can be estimated. For this purpose a $1 \times 10^{14}/cm^2$ sample has been used to study the temperature dependence of the resistivity after each annealing up to 800°C. Figure 4.7. gives the results.

The ionization energy of zinc in gallium arsenide is 0.024 eV (27). The variation shown in Figure 4.7. has an activation energy of 0.26 eV. This large difference in the observed activation energy and the theoretical zinc acceptor activation energy is a definite indication

of the deep lying defect centers. As already stated, the nature of the implantation damage and the effect of the subsequent annealing is quite complex. The deep lying level could behave as an acceptor or donor level. As explained later, the profile measurements strongly support the action of the defect centers as donors. In this case Appendix II shows the temperature dependence of resistivity to be

$$\rho \sim \frac{N_D}{N_{zn} N_v} \exp \frac{(E_D - E_v)}{KT} \qquad 4.1$$

In equation 4.1, N_D, the concentration of defects, and N_{zn}, the concentration of electrically active zinc impurities, are both functions of annealing temperature. From the variation shown in Figure 4.7 it is obvious that N_D has to increase faster than N_{zn} up to 400°C annealing and at higher annealing temperatures the electrically active zinc impurity centers increases much faster than the defect centers. This factor is not understood.

The effective surface resistivity as a function of 1000/T°K shown in Figure 4.7 shows a saturation at low temperatures. Moreover, the sheet resistivity changes by three orders of magnitude within about 60°C below room temperature. This is caused primarily by the drastic change in the carrier concentration. The mobility change is considerably less than an order of magnitude. If we assume that the defect centers act as donors, at low temperature $p \simeq N_{zn} - N_D = 1.4 \times 10^{16}/cm^3$. At room temperature $p \simeq [N_{zn} - N_D(1-f)] = 4.5 \times 10^{18}/cm^3$, where f is the fermi-dirac function evaluated at the donor energy. A rough, though not exact, estimate gives the number of defect centers to be greater than

$9.5 \times 10^{18}/cm^3$. The number of defect centers is rather high. Baron et. al (1) have reported the implantation of aluminum and bismuth in silicon and have suggested a model of compensating acceptor type defect centers. Their results show the concentration of the defect centers to be between $4 \times 10^{17}/cm^3$ and $1 \times 10^{19}/cm^3$. The concentration of the defect centers obtained in the present experiments is of the same magnitude as reported by Baron et. al (1). Under the assumption that the defects act as donor, the degree of compensation is very close to the zinc acceptors. It is hard to believe that such a close compensation is occurring. However, the profile measurements can be explained only by a donor model. The measurements and calculations of profile data were repeated and confirmed. So the donor model is chosen.

4.4 Profile Measurements

Extensive profile measurements have not been attempted, though they will give more information on the properties of the implanted layer. A profile estimate has been made on one sample of $1 \times 10^{15}/cm^2$ dose annealed at 800°C. The results are given in Figure 4.8. As stated previously, no accurate measurement of the thickness of the etched layers has been done. The thickness is estimated purely from the assumed etch rate. Formulae derived in Appendix-I are used to obtain the profile of mobility and the net active acceptor density, n_I/cm^3. The profile of the effective surface concentration N_s/cm^2 is obtained directly from the measurements using equation 3.6. These three profiles follow directly from the measured data and have no ambiguity attached except that there is approximately a 20% error

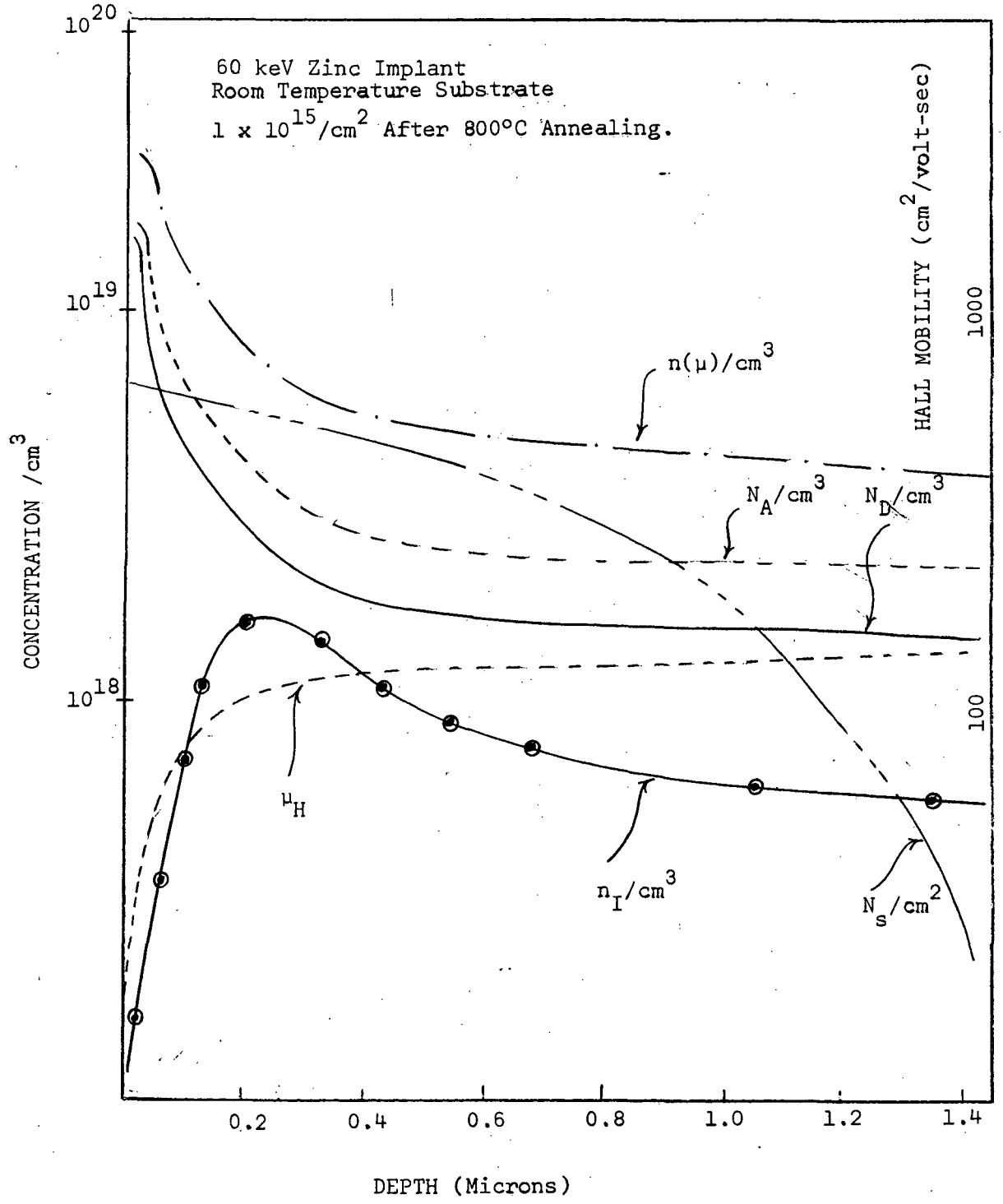

Figure 4.8. Mobility and different carrier concentration profiles of a 1×10^{15} /cm^2 dose implant after 800°C annealing.

due to the uncertainty of the etch rate.

The mobility was very low in the first 500 Å and increased to values of 120 cm^2 $volt^{-1}sec^{-1}$ deep in the implanted layers. The net active (acceptor) carrier density, n_I/cm^3, profile had a long tail and indicates that zinc has diffused to a depth of about 1·5μ. This $1 \times 10^{15}/cm^2$ implanted sample had an effective surface concentration of $3 \times 10^{14}/cm^2$ after 600°C annealing. Assuming this as a thin limited source of zinc and a diffusion coefficient of 5.5×10^{-10} cm^2 sec^{-1}(5), then from the measured surface concentration after 800°C annealing, zinc should have diffused to a depth of approximately 30μ for the 30 minutes annealing. But the measured depth was only about 1.5μ. Zinc has a diffusion coefficient highly dependent on concentration (5). As the diffusion proceeds from the implanted layer the concentration will decrease and result in a decreased depth. This is a possible reason for the low measured depth compared to the calculated one. The projected range of 60 keV zinc in gallium-arsenide is about 270 Å (14) while the measured depth is 1.5μ. This shows that diffusion of zinc has to be taken into consideration while implanting for any desired profile and concentration.

If we assume that the carrier scattering is caused by both the zinc acceptor impurities and the defect centers which are partially ionized at room temperature, the mobility profile can be used to estimate the total number of ionized centers. The profile named $n(\mu)/cm^3$ is the profile of the total number of ionized centers. The mobility versus surface carrier concentration curve given in Figure 4.4. has been used to obtain n(μ) profile, assuming a layer thickness of

1000 Å.

While discussing the resistivity vs temperature dependence the deep lying defect centers have been said to act as either a donor or an acceptor. If we examine the hypothesis that the defect centers have the effect of acceptors, then both n(μ) and n(I) should almost coincide at least deep in the layer. Because n(I), the total ionized impurity centers and n(I), the total ionized impurity centers and n(I), the total acceptors, are both given by $[N_{zn} + N_D(1-f)]$. In the present case the results of the profile measurements show them to be more than an order of magnitude apart. If we examine the hypothesis of donor centers compensating the zinc impurity, the results of the profile measurements could be explained. The n(μ) profile represents the total number of ionized impurity centers i.e. $[N_{zn} + N_D(1 - f)]$. While the n_I profile represents the net active acceptors i.e. $[N_{zn} - N_D(1 - F)]$. Since the two profiles represent the sum and difference of the zinc acceptors and donor type defect centers they lie one above the other. The area under n(μ) represents $7.64 \times 10^{14}/cm^2$ which is close to the initial implanted dose i.e. $1 \times 10^{15}/cm^2$. The total number of defects are $3.41 \times 10^{13}/cm^2$ which is of the same order as reported by Baron et. al. (1).

The results of the profile measurements support the model of compensating donor defect centers as influencing the electrical properties. However, the results of the profile measurements have several shortcomings. First of all, the thickness etched has not been measured accurately. Secondly, the n(μ) profile is directly deduced from the mobility profile. The mobility values near the surface is low and there could be many reasons for this. The presence of the surface could be

one reason. Whether it is justifiable to conclude the value of $n(\mu)$ from this mobility near the surface is questionable. The major contribution to the area under $n(\mu)$ comes from this area near the surface. Moreover, the $n(\mu)$ profile fails to show any peak as predicted by the L.S.S. theory. Again the compensation obtained is so close to the doping level that it is a little hard to believe the figures obtained. However, the profiles deep in the implanted layer support the compensation model in spite of the shortcomings near the surface. The measurements and the calculations were repeated several times to confirm the profile experimentally obtained.

CHAPTER V

SUMMARY, CONCLUSIONS AND RECOMMENDATIONS

5.1 Summary and Conclusions

The annealing characteristics of zinc implanted into semi-insulating gallium-arsenide have been studied. The substrate into which 60 keV zinc ions were implanted had resistivities of the order of 1×10^8 ohm-cm. This resistivity is the result of the compensating action of the chromium doping whose concentration was around $5 \times 10^{16}/cm^3$. Zinc was implanted at various fluence levels from $1 \times 10^{12}/cm^2$ to $1 \times 10^{15}/cm^2$ and the behavior of the electrical properties upon annealing has been studied.

In the as-implanted condition the resistivity was nearly independent of implantation dose. This resistivity is believed to be due to the lattice damage produced during implantation. There is no experimental evidence to this assumption. The sample with $10^{12}/cm^2$ dose had a higher as-implanted resistivity than other doses. This indicates that the initial lattice damage is not sufficiently large to overcome the compensating influence of the chromium atoms. Two different modes of the kinetics of the annealing of radiation damage were observed. The resistivity of samples with a $1 \times 10^{15}/cm^2$ dose decreased steadily upon annealing. For all other doses the sheet resistivity increased drastically and approached values near that of the substrate after 400°C annealing. This annealing effect has been associated with the removal of the initial lattice damage before many of the implanted atoms become electrically active. This indicates that very few of the implanted ions become electrically active until much of the radiation damage is removed.

Up to 400°C annealing the mobility values were around 10 cm^2/volt-sec. because the carriers are due to lattice damage only. At 400°C the mobility values increases to around 50 cm^2/volt-sec. This is an indication that a few of the implanted zinc ions are becoming electrically active.

Upon annealing to 600°C and 800°C, the resistivity decreases considerably and the mobility attains values that are comparable to those obtained by thermal diffusion. This is an indication that most of the implanted ions become electrically active after 600°C annealing. The high resistivity and low mobility of the sample with $1 \times 10^{12}/cm^2$ dose illustrates an important point. This point is that in order to obtain implanted layers in semi-insulating gallium-arsenide which are free from any influence of the substrate, the implanted dose should yield doping levels much greater than the chromium concentration. In the present case this was easily obtained by implantations above $1 \times 10^{13}/cm^2$. For doses above $1 \times 10^{13}/cm^2$ the final sheet resistivity was slightly dose dependent. The final value of sheet resistivity was between 5×10^3 to 1×10^4 ohm per square for doses between $1 \times 10^{13}/cm^2$ to $1 \times 10^{15}/cm^2$. There is little additional annealing after 600°C. In many cases 800°C annealing resulted in resistivities slightly higher than the 600°C annealing. This increase is believed to result from the diffusion of the implanted ions at 800°C. The profile measurements indicates this. In attempting to make p-n junctions by ion implantation this post implantation diffusion should be taken into consideration.

For doses above $1 \times 10^{14}/cm^2$ the effective surface concentration saturates at about $1 \times 10^{14}/cm^2$. For doses below this there is

essentially 100% electrical activity. This saturation effect could be due to the solid solubility. No exact profile measurement or actual range measurements were done to determine the depth to which the implanted ions are confined. Nothing can be conclusively said about the role of the solid solubility in limiting the carrier concentration at high doses. Baron, et. al., (1) have suggested that radiation defect centers or complexes could act as donors or acceptors and influence the net carrier concentration. The temperature dependence of resistivity clear-16 indicates such a defect center with an activation energy of 0.26 ev above balence band. The profile measurement indicates that the defect centers are donors.

Finally, the variation of mobility with temperature and its dependence on carrier concentration indicates that mobility is dominated by ionized impurity scattering after annealing above 400°C.

5.2 Recommendations

The high resistivity of the sample was always a problem in all the measurements. The noise was of the order of the signal in some cases. Probably, if an a.c. Hall-effect measurement technique is adopted this problem could be reduced.

More work has to be done to determine the actual cause of the carrier-concentration saturation effect at high doses. More extensive profile measurements, backscattering studies and electron-spin-resonance studies will give information on the location, nature and behavior of the implanted atoms.

CHAPTER VI

6. LIST OF REFERENCES

1. Baron, R., G. A. Shifrin, O. J. Marsh, and J. W. Mayer 1969. Electrical behaviour of group III and V implanted dopants in silicon. J. Appl. Phys. 40:3702.

2. Brooks, H., and C. Herring. 1951. Scattering by ionized impurities in semiconductors. Phys. Rev. 83:879.

3. Buehler, M. G. 1966. Stanford Res. Rept. SEL-66-004 July.

4. Carter, G., W. A. Grant, J. D. Huskell, and G. A. Stephens. 1970. Radiation damage by implanted ions in GaAs and GaP. Radiation Effects 6: 277-284.

5. Chang, Leory. L. 1963. Diffusion, solubility and distribution coefficient of zinc in gallium-arsenide and gallium-phosphide. Stanford Research - Reports. SEL. 63-104.

6. Davis, J. A., J. Denhartog, L. Eriksson and J. W. Mayer. 1967. Ion Implantation of Silicon. Can. J. Phys. 45: 4053-4089.

7. Foyt, A. G., J. P. Donnelly, and W. T. Lindley. 1969. Efficient doping of Ga As by Se^{+} ion implantation. Appl. Phys. Letters. 14(12):372.

8. Glotin, P. and J. Grapa. 1967 Conference on application of ion beams to semiconductors, Grenoble. Page 179.

9. Hunsperger, R. G., H. L. Dunlap, and O. J. Marsh. 1968. Development of Ion Implantation Techniques for microelectronics. Prepared under contract no. NAS 12-124 by Hughes Research Laboratories, Malibu, California. Annual Report - 1968.

10. Hunsperger, R. G., and O. J. Marsh. 1968. The presence of deep levels in ion implanted junctions. Appl. Phys. Letters. 13(9) : 295.

11. Hunsperger, R. G., and O. J. Marsh. 1969. Electrical properties of zinc and Cadmium Ion Implanted layers in Ga-As. J. Electrochemical Soc., 116(4) : 488-491.

12. Hunsperger, R., and O. J. Marsh. 1970. Electrical properties of Cadmium, Zinc and Sulfer ion implanted layers in Ga-As. Radiation Effects. 6 : 263-268.

13. Johansson, N. E. G., and J. W. Mayer. 1970. Technique used in Hall-effect analysis of ion implanted Silicon and Germanium. Solid State Electronics. 13: 317-335.

14. Johansson, W. S., and J. F. Gibbons, 1969. Projected Range Statistics in Semiconductors. Distributed by Stanford University Book Store.

15. Linhard, J., and M. Scharff. 1961. Energy Dissipation by Ions in the keV Region. Phys Rev 124: 128.

16. Manchester, K. E. 1966. The Art of Semiconductor Doping by Ion Implantation. Solid State Technology. September 1966 : 48-52

17. Marsh, O. J., H. Dunlap, R. Hart, and R. G. Hunsperger. 1969 : Development of ion implantation technique for microelectronics. Final Report of Contract No. NAS 12-124 by Hughes Research Laboratories, Malibu, California.

18. Marsh, O. J., R. G. Hunsperger, H. L. Dunlap, and J. W. Mayer 1967: Development of ion implantation technique for microelectronics. Annual Report 1967. Prepared under Contract No. NAS 12-124 by Hughes Research Laboratories. Malibu, Calif.

19. Mayer, J. W., L. Eriksson, and J. A. Davis. 1970. Ion implantation in semiconductors. Silicon and Germanium. Academic Press. N. Y. 1970.

20. Mayer, J. W., O. J. Marsh, R. Mankarious, and R. Bower. 1967. Zinc and Tellurium implantations into Gallium-Arsenide. J. Appl. Phys. 38 : 1975-76.

21. Petritz, R. L., 1958. Theory of an experiment for measuring the mobility and density of carriers in the space charge region of a semiconductor. Phys. Rev. 110(6) : 1254.

22. Putley, E. H. 1960. The Hall-effect and Semiconductor Physics. Dover Publications, Inc. N. Y.

23. Rossi, F., D. Meyerhoffer, and R. Jensen. 1959. Properties of p- type Ga As prepared by Copper diffusion. J. Appl. Phys. 31 (6) : 1105-1108.

24. Sansbury, J. D., and J. F. Gibbons. 1969. Conductivity and Hall mobility of ion implanted silicon in semi-insulating gallium-arsenide. Appl. Phys. Letters. 14(10) : 311-315.

25. Sansbury, J. D., and J. F. Gibbons. 1970. Properties of ion implanted Silicon, Sulpher and carbon in gallium arsenide. Radiation Effects 6 : 269-276.

26. Sze, S. M. 1969. Physics of Semiconductor Devices. John Wiley. N. Y. Page 40.

27. Sze, S. M., and J. C. Irvin. 1968. Resistivity, mobility and impurity levels in Ga As, Ge, and Si at 300°K. Solid State Electronics. 11 : 599-602.

28. Van der Pauw, L. J. 1958. A method of measuring specific resistivity and Hall-effect of discs of arbitrary shape. Philips. Res. Repts. 13:1.

29. Westmoreland, J. E., O. J. Marsh, and R. G. Hunsperger. 1970. Lattice disorder produced in Ga As by 60 KeV Cd-ions and 70 KeV Zn - ions. Radiation Effects. 5 : 245-249.

CHAPTER VII

7. APPENDICES.

7.1 Appendix-1 Formula Used in the Analysis of the Layer Removal Technique

When both carrier concentration and mobility are functions of depth, the sheet conductivity and sheet Hall coefficient - the quantities actually measured - are weighted averages. R. L. Petritz (21) has derived the following formulae for the sheet Hall coefficient R_{HS} and sheet conductivity, σ_s.

$$R_{HS} = \int n(x) < \mu(x)^2 > dx/e \left[\int n(x) < \mu(x) > dx \right]^2 \qquad 7.1$$

and

$$\sigma_s = e \int n(x) < \mu(x) > dx \qquad 7.2$$

Where $n(x)$ and $\mu(x)$ are the carrier concentration and mobility at distance x perpendicular to surface and e in the electronic charge. Since the implanted layer is thin the above formulae are applicable to implanted layer. Buehler (3) has extended the work of Petritz and according to him solving and differentiating the above equations give

$$e\, n(x) < \mu(x) > = d\sigma_s/dx \qquad 7.3$$

$$e\, n(x) < \mu(x)^2 > = \frac{d(R_{HS}\sigma_s^2)}{dx} \qquad 7.4$$

These two equations can in turn be solved for the hall mobility and density distribution to give

$$\mu_H(x) = \frac{d(R_{HS}\sigma_s^2)}{dx} \Big/ \frac{d\sigma s}{dx} \qquad 7.5$$

and

$$n(x) = \frac{\mu_h(x)}{e\mu_c(x)} \left(\frac{d\sigma_s}{dx}\right)^2 \Big/ \frac{d(R_{hs}\sigma^2{}_s)}{dx} \qquad 7.6$$

Since μ_h/μ_c is normally equal to unity no correction for $\mu_h(x) / \mu_c(x)$ is applied.

Experimentally the distributions are determined by measuring R_{HS} and σ_s after each successive removal of thin layer of material as explained previously. The derivatives are approximated by

$$\frac{d\sigma_s}{dx} = \frac{\Delta(\sigma_s)_i}{\Delta x_i} \qquad 7.7$$

and

$$\frac{d(R_{hs}\sigma_s^2)}{dx} = \frac{\Delta(R_{hs}\sigma_s^2)\, i}{\Delta x_i} \qquad 7.8$$

Here Δx_i is the thickness of the material removed in the i^{th} strip and $\Delta(\sigma_s)_i$ and $\Delta(R_{hs}\sigma_s^2)i$ are the changes in these quantities by the i^{th} strip.

7.2 Appendix-II Resistivity dependence on temperature

It is desired to obtain a relation between the resistivity and temperature. The zinc-acceptor impurity is assumed to be influenced by deep lying defect centers. The profile measurements indicate that the defect centers could act as deep donors acting as compensating centers. If the defect centers have a concentration N_D at an energy level E_D in the upper half of the band gap, then at high temperatures the hole concentration, p, is given by

$$p = N_{Zn} - N_D \left[1 - f(E_D)\right] \qquad 7.9$$

where $f(E_D)$ is the Fermi-Dirac distribution function.

Also,

$$p = N_v \exp -\left(\frac{E_f - E_v}{KT}\right) . \qquad 7.10$$

If $N_D >> N_{Zn}$,

then $$\left[1 + \exp\left(\frac{E_f - E_D}{KT}\right)\right]^{-1} \simeq \exp - \left[\frac{E_f - E_D}{KT}\right]$$

Thus

$$p = N_{Zn} - N_D \exp - \left(\frac{E_f - E_D}{KT}\right) \qquad 7.11$$

$$= N_v \exp - \left(\frac{E_f - E_v}{KT}\right) \qquad 7.12$$

Let $(E_F - E_V) / KT = E_k$ and $(E_D - E_V) / KT = E_d$

Solving for E_k from equations 7.11 and 7.12 give

$$\exp(-E_k) = \frac{N_{Zn}}{N_V + N_D \exp(E_d)} \qquad 7.13$$

Equation 7.11 can be written as

$$p = N_{Zn} - N_D \exp(-E_k) . \exp(E_d)$$

Now substituting for $\exp(-E_k)$ gives

$$p = \frac{N_{Zn} N_V}{N_V + N_D \exp(E_d)}$$

Since $N_D >> N_V$

$$p \simeq \frac{N_{Zn} N_V}{N_D} \exp(-E_d)$$

and

$$1/p \simeq \frac{N_D}{N_{Zn} N_V} \exp\left(\frac{E_D - E_V}{KT}\right)$$

The change of mobility with temperature is far less compared to the change in the number of hole. Hence the resistivity should change with temperature approximately as

$$\rho \propto \frac{N_D}{N_{Zn} N_V} \exp\left(\frac{E_D - E_V}{KT}\right) . \qquad 7.14$$